^{13}C–^{1}H dipolar-driven ^{13}C–^{13}C recoupling without ^{13}C rf irradiation in nuclear magnetic resonance of rotating solids

K. Takegoshi, Shinji Nakamura, and Takehiko Terao
Department of Chemistry, Graduate School of Science, Kyoto University, Kyoto 606-8502, Japan

Two recently proposed ^{13}C–^{13}C recoupling methods under magic angle spinning (MAS), resonant interference recoupling (RIR), and ^{13}C–^{1}H dipolar-assisted rotational resonance (DARR), are examined on a common theoretical foundation using the average Hamiltonian theory. In both methods, a rf field is applied on not ^{13}C but ^{1}H to recouple the ^{13}C–^{1}H dipolar interactions, and spectral overlap necessary to conserve energy for ^{13}C–^{13}C polarization transfer is achieved by the ^{13}C–^{1}H dipolar line broadening. While DARR employs time-independent ^{13}C–^{1}H interactions recoupled by suitable rf irradiation to ^{1}H spins, RIR uses time-dependent ^{13}C–^{1}H interactions modulated appropriately by ^{1}H rf irradiation. There are two distinct cases where ^{13}C–^{1}H line broadening realizes ^{13}C–^{13}C spectral overlap. For a pair of a carbonyl or aromatic carbon and an aliphatic carbon, spectral overlap can be achieved between one of the spinning sidebands of the former ^{13}C resonance and the ^{13}C–^{1}H dipolar powder pattern of the latter. On the other hand for a pair of spins with a small chemical shift difference, the two center bands are overlapped with each other due to ^{13}C–^{1}H dipolar broadening. For the former, we show that both RIR and DARR occur in the first order, while for the latter, DARR recoupling is appreciable for time-independent ^{13}C–^{1}H interactions. We refer to the former DARR as the first-order DARR recoupling and the latter as the second-order DARR. Experimentally, we examined the following ^{13}C–^{1}H recoupling methods for DARR: ^{1}H CW irradiation fulfilling a rotary-resonance condition or a modulatory-resonance condition, and ^{1}H π pulses applied synchronously to MAS. For RIR, the FSLG-$m\overline{2}mm$ sequence is applied to ^{1}H. Several one-dimensional DARR and RIR experiments were done for N-acetyl[1,2-^{13}C, ^{15}N] DL-valine, and [2,3-^{13}C] L-alanine. It was found that the polarization transfer rate for RIR is larger than that for DARR except for fast spinning, while the rate for DARR is less sensitive to the spinning speed. Further, we showed that the efficiency of the second-order DARR recoupling is not significantly less than that of the first-order DARR. Among the ^{13}C–^{1}H recoupling methods examined, CW irradiation at the $n=1$ rotary-resonance condition is superior for DARR because it gives a larger ^{13}C–^{1}H dipolar broadening, leading to broadband recoupling. We showed that a broadband-recoupling experiment with the first and the second-order DARR by CW irradiation at the $n=1$ rotary-resonance condition is applicable to signal assignment as well as structural determination of a multiply/uniformly ^{13}C labeled molecule as demonstrated by two-dimensional ^{13}C–^{13}C DARR polarization-transfer experiments of uniformly ^{13}C, ^{15}N-labeled glycylisoleucine. © *2003 American Institute of Physics.* [DOI: 10.1063/1.1534105]

I. INTRODUCTION

Polarization transfer among homonuclear spins, being often referred to as spin diffusion after the pioneering work done by Bloembergen,[1] is a long-standing subject in NMR and has been extensively investigated both theoretically and experimentally.[2] This is because polarization transfer plays an important role in many aspects of NMR. For example, fast spin diffusion among ^{1}H spins in solids enables the ^{1}H spin system to reach the internal thermal equilibrium in a short time so that one can apply thermodynamics to describe its behavior such as relaxation. Efficient polarization transfer requires the total spin polarization to be conserved and simultaneous spin flip–flop motion or flop–flop motion to occur. Both are satisfied for ^{1}H spins in solids, whose resonance frequencies are degenerated and the dipolar couplings are strong. However, polarization transfer becomes less efficient for spins having a smaller gyromagnetic ratio (γ), such

as ^{13}C, because of the smaller homonuclear dipolar couplings. Further, spectral overlap necessary for energy conservation is not always fulfilled for ^{13}C spins because of the large variation of isotropic chemical shifts. In addition to these, magic-angle spinning (MAS) of samples, which is indispensable for high-resolution observation, hinders efficient transfer by removing the ^{13}C–^{13}C dipolar interaction.

So far, a variety of techniques for polarization transfer among low-γ nuclei such as ^{13}C under MAS have been proposed; they can be classified into four categories according to the source of compensating the energy mismatch in highly resolved resonances:[2] (1) ^{1}H-driven, (2) motionally driven, (3) rf-driven, and (4) rotor-driven. The ^{1}H-driven method employs line broadening by ^{13}C–^{1}H dipolar couplings, which provides a mechanism of energy matching for a pair of ^{13}C spins with the chemical-shift difference is comparable to or smaller than the line broadening. Since the ^{13}C–^{13}C

2325

dipolar interactions removed by MAS are not recovered in the first order for the ^{1}H-driven method, its efficiency is low in particular at fast MAS speeds. The motionally driven mechanism works only when molecular motion with a proper correlation time exists, thus this cannot be applied in general. A number of the rf-driven polarization transfer methods using various ^{13}C rf-pulse sequences have been proposed to realize the dipolar recoupling and the energy matching simultaneously under MAS, to name a few examples, RFDR,[3] HORROR,[4] CROWN,[5] C7,[6] and R2TR.[7] For these rf-driven methods employing ^{13}C rf irradiation, ^{13}C magnetization decays rapidly due both to inhomogeneity of the rf field and to a short relaxation time under a rf field. Therefore, it is difficult to determine a long internuclear distance using a rf-driven method. This drawback in the rf-driven experiments is absent for the rotor-driven experiment based on rotational resonance (R^2) (Refs. 8–15) recoupling.

For R^2, the flip–flop term for the pair of spins can be reintroduced by matching an integral multiple of the MAS frequency (ν_R) to the difference of the isotropic chemical shifts between a pair of low-γ spins such as ^{13}C ($\Delta = n\nu_R$: the R^2 condition). Since no rf field is applied to ^{13}C spins, the process competitive against polarization transfer is a generally long ^{13}C spin-lattice relaxation process. The R^2 method is, therefore, suitable to cause polarization transfer between a specific pair of ^{13}C spins with a proper chemical shift difference, and, in fact, used to obtain a crucial internuclear distance in some selectively pair-labeled biomolecules.[16] However, for a pair whose chemical shift difference is smaller than their chemical shift anisotropies (CSA), the R^2 condition imposes slow spinning leading to a number of spinning side bands. Further, under the R^2 condition, the line shapes of the paired ^{13}C spins exhibit characteristic patterns due to the recoupled ^{13}C–^{13}C dipolar interaction. Therefore, advantages of high resolution under MAS cannot fully be appreciated for the R^2 method.

Recently, we present two polarization transfer methods of resonant interference recoupling (RIR) (Ref. 17) and ^{13}C–^{1}H dipolar-assisted rotational resonance (DARR),[18] which have the following desirable features: (1) no rf irradiation to ^{13}C, (2) less restriction for the spinning speed, and (3) high resolution during observation. The underlying recoupling mechanism for these methods is common and can be classified as a combined mechanism of ^{1}H-driven and rotor-driven recoupling, because the extra energy necessary to cause the ^{13}C–^{13}C flip–flop transition is provided from the ^{1}H reservoir as well as macroscopic sample rotation (MAS). Here, we refer to the mechanism of DARR and RIR as ^{13}C–^{1}H dipolar-driven recoupling. One salient feature of the ^{13}C–^{1}H dipolar-driven method is the active use of the ^{13}C–^{1}H dipolar interaction. For the conventional ^{1}H-driven mechanism, the ^{13}C–^{1}H dipolar interaction is introduced by simply turning off the ^{1}H decoupling field. This brings homogeneous line-broadening due to ^{13}C–^{1}H and ^{1}H–^{1}H dipolar interactions, which allows a pair of ^{13}C resonances with different chemical shifts to overlap with each other, provided that the chemical shift difference is smaller than the sum of the line-broadenings.

In DARR, the ^{13}C–^{1}H dipolar interaction is recovered by suitable rf irradiation on ^{1}H, for example, by ^{1}H irradiation with the intensity ν_1 satisfying the rotary-resonance condition $\nu_1 = n\nu_R$ ($n = 1$ or 2).[19] The spectral overlap between the two relevant ^{13}C spins is realized between a spinning sideband of one ^{13}C spin and the ^{13}C–^{1}H dipolar pattern of the other ^{13}C spin and vice versa. Then, recoupling due to rotational resonance occurs for the ^{13}C–^{13}C pair, leading to facile polarization transfer under MAS. In RIR, the ^{13}C–^{1}H dipolar interaction is not recovered but modulated by applying the FSLG-$m\overline{2}mm$ sequence[20] to ^{1}H. It is noted that, unlike ^{1}H-driven and DARR, ^{1}H–^{1}H dipolar interactions are removed. Under FSLG-$m\overline{2}mm$ and MAS, the ^{13}C–^{1}H dipolar interactions become *inhomogeneous* with its spin part being modulated by FSLG-$m\overline{2}mm$ and its spatial part by MAS. On the other hand, the spin part of the ^{13}C–^{13}C dipolar interaction is modulated by the chemical shift difference, and the spatial part by MAS. Since the ^{13}C–^{1}H and ^{13}C–^{13}C dipolar Hamiltonians are not commutable, they are interfered with each other. It is shown that when the modulation frequencies for the ^{13}C–^{1}H and ^{13}C–^{13}C dipolar interactions are matched, a time-independent ^{13}C–^{13}C flip–flop term is recovered. The matching of modulation frequencies is made by properly choosing a cycle time for FSLG-$m\overline{2}mm$. Similarly to R^2, the ^{13}C–^{1}H dipolar-driven methods (RIR and DARR) do not have the short decay problem associated with rf irradiation on ^{13}C. Hence, in ^{13}C–^{13}C polarization-transfer experiments the polarization-transfer time is only limited by a generally long ^{13}C spin-lattice relaxation time. This makes it possible to realize long-range ^{13}C–^{13}C polarization transfer.

In this work, we develop a common theoretical framework to describe RIR and DARR. It is shown that RIR is frequency-selective recoupling, while DARR is frequency- and orientation-selective recoupling with its selectivity being relaxed/deteriorated by the homogeneous broadening due to nonaveraged ^{1}H–^{1}H dipolar couplings. For a commonly used static magnetic field and a spinning speed of a few 10 kHz, DARR and RIR can be used to recouple carboxyl/carbonyl/aromatic carbons and aliphatic carbons. Further, we theoretically show that in the second order, DARR recoupling does occur even between the resonances with a smaller chemical shift difference typically in aliphatic carbons. Hence, broadband recoupling is achieved by DARR. In fact, recently we showed that broadband polarization transfer by DARR occurs in the Nuclear Overhauser Polarization (NOP) experiment, where ^{1}H irradiation of DARR causes ^{13}C signal enhancement based on the nuclear Overhauser effect not only for ^{13}C of fast rotating methyl groups but also for the other ^{13}C spins in a fully ^{13}C labeled peptide sample.[21] The uniform enhancement of the nonmethyl carbons is attributed to broadband polarization transfer from the methyl carbons to them. Interestingly, it was pointed out that the ^{13}C–^{13}C transfer rates from the methyl carbons to the other carbons correlate well with the ^{13}C–^{13}C distances. This indicates a possibility of determining internuclear distances roughly by the polarization transfer experiment under DARR. While R^2 causes line broadening and therefore spoils the advantage of high resolution, the present ^{13}C–^{1}H dipolar-driven method can fully appreciate high resolution when combined with

multidimensional NMR. Further, DARR does not require any critical adjustments of experimental settings. We show that these features of DARR are useful for the signal assignments as well as the structure determination of multiply ^{13}C-labeled peptides.

II. THEORY

We consider a system composed of two dipolar-coupled ^{13}C spins (S_1 and S_2) and one ^{1}H (I) spin under MAS and rf irradiation on ^{1}H. The other abundant ^{1}H spins are ignored for both RIR and DARR due to the following reasons. For RIR, we remove the ^{1}H–^{1}H dipolar interactions by the FSLG-$m\overline{2}mm$ irradiation[20] on the ^{1}H spin. For DARR, the homogeneous broadening originated from the other ^{1}H spins increases the efficiency of the ^{13}C–^{13}C polarization transfer, but does not directly relate to the ^{13}C–^{13}C recoupling mechanism.[18] For simplicity, we further neglect the chemical shift anisotropy (CSA) interactions.

A. Spin Hamiltonians under MAS and time evolution

The total spin Hamiltonian consists of the Zeeman interaction $\mathcal{H}_Z(t)$, the ^{13}C–^{1}H dipolar interaction $\mathcal{H}_D^{IS}(t)$, and the ^{13}C–^{13}C dipolar interaction $\mathcal{H}_D^{SS}(t)$,

$$\mathcal{H}_{\text{total}} = \mathcal{H}_Z(t) + \mathcal{H}_D^{IS}(t) + \mathcal{H}_D^{SS}(t). \tag{1}$$

In the frame rotating at the Larmor frequencies of ^{1}H and ^{13}C spins (the double rotating frame), the Zeeman interaction is given by

$$\mathcal{H}_Z(t) = \mathcal{H}_Z^S + \mathcal{H}_Z^I(t) \tag{2}$$

with

$$\mathcal{H}_Z^S = \delta_1 S_{z1} + \delta_2 S_{z2},$$

$$\mathcal{H}_Z^I(t) = \delta(t)I_z + \nu_1(t)\{I_x \cos \phi(t) + I_y \sin \phi(t)\}, \tag{3}$$

where δ_i is the isotropic chemical shift of the ^{13}C$_i$ spin (i =1,2). For the ^{1}H spin, we consider that the resonance offset $\delta(t)$, the intensity $\nu_1(t)$, and the phase $\phi(t)$ of a ^{1}H rf field are time dependent for generality. For the homonuclear ^{13}C–^{13}C dipolar interaction under MAS, we have

$$\mathcal{H}_D^{SS}(t) = d(t)\{S_{1z}S_{2z} - \tfrac{1}{4}(S_{1+}S_{2-} + S_{1-}S_{2+})\} \tag{4}$$

with

$$d(t) = g_1 \cos(2\pi\nu_R t + \gamma) + g_2 \cos(4\pi\nu_R t + 2\gamma), \tag{5}$$

$$g_1 = \frac{3d_0}{2} \sin 2\theta_M \sin 2\beta, \tag{6}$$

$$g_2 = -\frac{3d_0}{2} \sin^2 \theta_M \sin^2 \beta. \tag{7}$$

Here, d_0 is the dipolar coupling constant $(\mu_0/4\pi)$ $\times(\gamma_S^2\hbar/r_0^3)$, ν_R is the sample spinning speed, and θ_M is the magic angle. β and γ describe the orientation of the ^{13}C$_1$–^{13}C$_2$ internuclear vector in the rotor-fixed frame. The heteronuclear dipolar Hamiltonian for the ^{13}C$_i$–^{1}H pair can be given in the double rotating frame by

$$\mathcal{H}_D^{IS_i}(t) = D_i(t)I_z S_{iz}, \tag{8}$$

where the geometric part $D(t)$ is written as

$$D_i(t) = G_{i1} \cos(2\pi\nu_R t + \gamma_i) + G_{i2} \cos(4\pi\nu_R t + 2\gamma_i) \tag{9}$$

with

$$G_{i1} = \frac{3d_i}{2} \sin 2\theta_M \sin 2\beta_i, \tag{10}$$

$$G_{i2} = -\frac{3d_i}{2} \sin^2 \theta_M \sin^2 \beta_i. \tag{11}$$

Here, β_i and γ_i describe the orientation of the ^{13}C$_i$–^{1}H internuclear vector in the rotor-fixed frame, and d_i is the dipolar coupling constant $(\mu_0/4\pi)(\gamma_I\gamma_S\hbar/r_i^3)$.

To appreciate the effects of the Zeeman interaction on the dipolar interactions, we transfer the dipolar interactions into the double interaction frame defined by the following unitary transformation:

$$U_Z(t) = U_S(t)U_I(t) \tag{12}$$

with

$$U_S(t) = \exp(-2\pi i\mathcal{H}_Z^S t),$$

$$U_I(t) = T \exp\left\{-2\pi i \int_0^t \mathcal{H}_Z^I(t')dt'\right\}, \tag{13}$$

where T denotes the Dyson time-ordering operator. The time-evolution operator in the double rotating frame can thus be written as

$$U(t) = T \exp\left\{-2\pi i \int_0^t \mathcal{H}_{\text{total}}(t')dt'\right\}$$

$$= U_Z(t)U_d(t)$$

with

$$U_d(t) = T \exp\left\{-2\pi i \int_0^t (\mathcal{H}_D^{IS*}(t') + \mathcal{H}_D^{SS*}(t'))dt'\right\}, \tag{14}$$

where the dipolar interactions in the double interaction frame is given by

$$\mathcal{H}_D^{IS*}(t) = U_I^{-1}(t)\mathcal{H}_D^{IS}(t)U_I(t)$$

$$= \sum_i D_i(t)S_{iz}U_I^{-1}(t)I_z U_I(t) \tag{15}$$

and

$$\mathcal{H}_D^{SS*}(t) = U_S^{-1}(t)\mathcal{H}_D^{SS}(t)U_S(t)$$

$$= d(t)[S_{1z}S_{2z} - \tfrac{1}{4}\{S_{1+}S_{2-} \exp(2\pi i\Delta t)$$

$$+ S_{1-}S_{2+} \exp(-2\pi i\Delta t)\}], \tag{16}$$

where $\Delta = \delta_1 - \delta_2$ is the chemical shift difference of the two ^{13}C spins. Hereafter, we neglect the $S_{1z}S_{2z}$ term because it is irrelevant to ^{13}C–^{13}C polarization transfer.

To appreciate ^{13}C–^{13}C recoupling, we isolate the ^{13}C–^{13}C dipolar Hamiltonian in Eq. (14) using two approaches. In one approach, the effect of $\mathcal{H}_D^{IS*}(t)$ on $\mathcal{H}_D^{SS*}(t)$ is calculated directly as

$$\widetilde{\mathcal{H}_D}^{SS*}(t) = U_{IS}^{-1}(t)\mathcal{H}_D^{SS*}(t)U_{IS}(t) \tag{17}$$

with

$$U_{IS}(t) = T \exp\left\{-2\pi i \int_0^t \mathcal{H}_D^{IS*}(t')dt'\right\}. \tag{18}$$

Desired $^{13}C-^{13}C$ recoupling is achieved for a certain $U_{IS}(t)$, which leads to a time-independent average Hamiltonian[22] as $\widetilde{\mathcal{H}_D^{SS*}}(t) \sim \overline{\mathcal{H}_D^{SS*}(0)}$. The time-evolution operator in the double rotating frame is then written as

$$U(t) = U_Z(t)U_{IS}(t)U_{SS}(t)$$

with

$$U_{SS}(t) = T \exp\left\{-2\pi i \int_0^t \widetilde{\mathcal{H}_D^{SS*}}(t')dt'\right\}$$

$$\sim \exp(-2\pi i \overline{\widetilde{\mathcal{H}_D^{SS*}(0)}}t). \tag{19}$$

This approach is particularly useful when a time-independent zeroth-order average Hamiltonian for the $^{13}C-^{1}H$ dipolar interaction can be obtained, so that we have

$$U_{IS}(t) \sim \exp\{-2\pi i \overline{\mathcal{H}_D^{IS*}(0)}t\}. \tag{20}$$

The other approach is to evaluate average Hamiltonians for $\mathcal{H}_D^{IS*}(t) + \mathcal{H}_D^{SS*}(t)$. To appreciate recoupling of the $^{13}C-^{13}C$ dipolar interaction, we apply the secular average Hamiltonian theory,[23] where the sum of time-dependent dipolar Hamiltonians is expressed by a Fourier series as

$$\mathcal{H}_D^{IS*}(t) + \mathcal{H}_D^{SS*}(t) = \sum H_n \exp(i2\pi \nu_n t), \tag{21}$$

and the zeroth and the first order average Hamiltonians are given as follows:

$$\mathcal{H}^{(0)} = H_0,$$

$$\mathcal{H}^{(1)} = \sum_{k>0} \frac{1}{2\pi \nu_k}[H_k, H_{-k}]. \tag{22}$$

This shows that if $\mathcal{H}_D^{IS*}(t)$ and $\mathcal{H}_D^{SS*}(t)$ have common Fourier components, they will give the time-independent first-order secular average Hamiltonian. The time-evolution is written in this case as

$$U(t) = U_Z(t)U_d(t)$$

with

$$U_d(t) \sim \exp\left(-2\pi i \sum \mathcal{H}^{(n)}t\right). \tag{23}$$

Comparison of these two approaches is made in the Appendix, and the latter secular average Hamiltonian is shown to be a good approximation of the former average Hamiltonian when the common modulation frequency ν_k exceeds the size of the time-dependent Hamiltonians.

B. A simple example: ^1H CW irradiation

To appreciate the effects of ^1H rf irradiation on the $^{13}C-^{13}C$ dipolar interaction under MAS, we take up on-resonance CW irradiation [$\nu_1(t)=\nu_1$, $\delta(t)=\delta$, and $\phi(t)=0$ in Eq. (3)] as a simple example. After straightforward calculation, we have

$$\mathcal{H}_D^{IS*}(t) = \sum_i D_i(t)S_{iz}\{I_z \cos(2\pi \nu_1 t) - I_y \sin(2\pi \nu_1 t)\} \tag{24}$$

in the double interaction frame. For simplicity, we assume that the $^{13}C_2-^1H$ dipolar interaction is negligible, $d_2 \sim 0$. The $^{13}C-^1H$ dipolar interaction is then written as

$$\mathcal{H}_D^{IS*}(t) = \sum_{n=1,2} G_{1n} \cos(2\pi n \nu_R t + n\gamma_1)$$

$$\times S_{1z}\{I_z \cos(2\pi \nu_1 t) - I_y \sin(2\pi \nu_1 t)\}$$

$$= \sum_{n=1,2} \frac{G_{1n}}{2} S_{1z}[I_z\{\cos(\Sigma_n t + n\gamma_1)$$

$$+ \cos(\Delta_n t + n\gamma_1)\} - I_y\{\sin(\Sigma_n t + n\gamma_1)$$

$$- \sin(\Delta_n t + n\gamma_1)\}] \tag{25}$$

with

$$\Delta_n = 2\pi(n\nu_R - \nu_1),$$

$$\Sigma_n = 2\pi(n\nu_R + \nu_1). \tag{26}$$

Note that the $^{13}C-^1H$ dipolar interaction is recovered at the following rotary-resonance recoupling condition,

$$\nu_1 = n\nu_R. \tag{27}$$

1. $^{13}C-^1H$ dipolar-assisted rotational resonance (DARR) by CW irradiation

Under the $n=1$ rotary-resonance condition ($\Delta_1=0$), we neglect the fast oscillating terms with $\Sigma_{n=1,2}$ and Δ_2 in Eq. (25). Then, we have the following zeroth order average Hamiltonian for the $^{13}C-^1H$ dipolar interaction,

$$\overline{\mathcal{H}_D^{IS*(0)}} = \frac{G_{11}}{2} S_{1z}(I_z \cos \gamma_1 + I_y \sin \gamma_1). \tag{28}$$

The resonance of the ^{13}C spin appears as a doublet at $\delta_1 \pm \frac{1}{4}G_{11}$ by this recoupling.[19] Here, we adopt the direct approach [Eqs. (17)–(20)] to appreciate the effects of $\mathcal{H}_D^{IS*}$ on $\mathcal{H}_D^{SS*}$ with the unitary operator $U_{IS}(t)$ [Eqs. (20)] being given using Eq. (28) as

$$U_{IS}(t) \sim U_X^{-1} \exp\left(-2\pi i \frac{G_{11}}{2} S_{1z}I_z t\right)U_X \tag{29}$$

with

$$U_X = \exp(-i\gamma_1 I_x). \tag{30}$$

The $^{13}C-^{13}C$ dipolar interaction modulated by the $^{13}C-^1H$ dipolar interaction [Eq. (17)] is then calculated to be

$$\widetilde{\mathcal{H}_D}^{SS*}(t) = -\frac{d_0}{8}\sum_{m=\pm 1,\pm 2} g_{|m|}\{S_{1+}S_{2-}\exp(2\pi iA_m t)$$

$$+ S_{1-}S_{2+}\exp(-2\pi iA_m t)\} \tag{31}$$

with

J. Chem. Phys., Vol. 118, No. 5, 1 February 2003

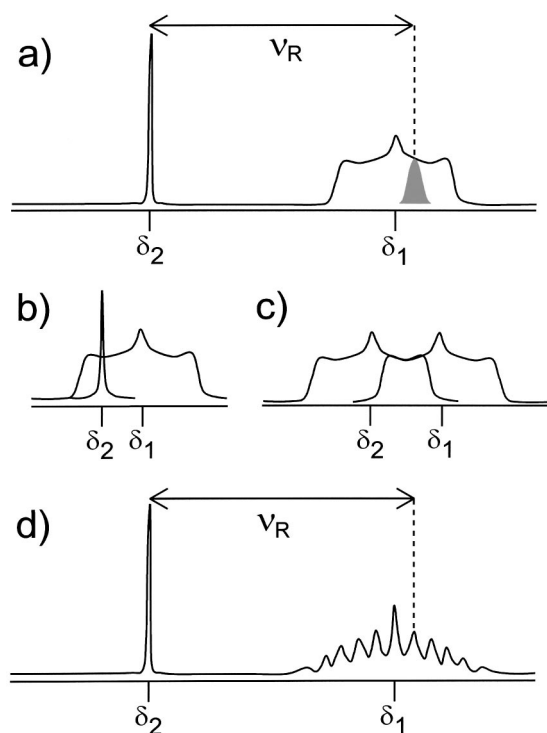^{13}C–^{1}H dipolar-driven ^{13}C–^{13}C recoupling   2329

a)

FIG. 1. Schematic ^{13}C MAS spectra of two ^{13}C spins under ^{13}C–^{1}H recoupling, showing various types of spectral overlap necessary for energy conservation in ^{13}C–^{13}C polarization transfer. Spectrum (a) represents two resonances of ^{13}CH at δ_1 and ^{13}C=O at δ_2. The hatched peak denotes one of the spinning sidebands of the ^{13}C=O peak, being overlapped with the recovered ^{13}C–^{1}H dipolar powder pattern of the ^{13}CH resonance. Spectrum (b) shows spectral overlap for a pair of spins whose chemical shift difference is smaller than the ^{13}C–^{1}H dipolar broadening. Spectrum (c) shows the case when spectral overlap occurs between two ^{13}C–^{1}H dipolar powder patterns. Spectrum (d) is similar to (a), but the ^{13}CH resonance shows a sideband pattern induced by modulation of the ^{13}C–^{1}H dipolar interaction under suitable ^{1}H rf irradiation. Spectral overlap is achieved for one of the spinning sidebands of the ^{13}C=O peak and one of the modulation-induced sidebands of the ^{13}CH resonance. The vertical dotted lines denote the position of the spinning sideband of the ^{13}C=O peak.

$$A_m = \Delta \pm \frac{G_{11}}{4} + m\nu_R. \tag{32}$$

Since the operator U_X has no effect on the ^{13}C–^{13}C dipolar interaction, I_z was replaced by $\pm 1/2$. Equation (31) indicates that ^{13}C–^{13}C recoupling is achieved when $A_m = 0$. It is worthy to note that in the conventional rotational resonance (R^2),[8–15] ^{1}H decoupling applied eliminates G_{11}, hence R^2 recoupling occurs at $\Delta = m\nu_R$. In the present case, the non-zero ^{13}C–^{1}H dipolar coupling modifies the conventional R^2 condition as

$$\Delta \pm \frac{G_{11}}{4} = m\nu_R. \tag{33}$$

This corresponds to a situation that one of the spinning sidebands of ^{13}C$_2$ is overlapped to the ^{13}C–^{1}H dipolar powder pattern of ^{13}C$_1$ as illustrated in Fig. 1(a). We refer to this recoupling as ^{13}C–^{1}H dipolar-assisted rotational resonance (DARR) recoupling. It should be mentioned here that similar DARR recoupling can take place also under the $n = 2$ rotary resonance condition. Further, the other heteronuclear dipolar

recoupling methods, such as modulatory-resonance recoupling (MORE) (Ref. 24) can also be used for DARR. Experimental examination of DARR by rotary resonance, by MORE, and by π pulses will be presented later.

2. The second-order DARR by CW irradiation

For a directly bonded ^{13}C–^{1}H spin pair, the maximum breadth of the ^{13}C doublet is ca. ± 7 kHz. Hence, Eq. (33) indicates that DARR does not occur for a pair whose chemical shift difference Δ is smaller than $\nu_R - 7$ kHz. For such a pair, however, spectral overlap may occur between the center band of one of the ^{13}C spin (S_2) and the ^{13}C–^{1}H dipolar-broadened resonance of the other (S_1) as illustrated in Fig. 1(b), showing the possibility of energy conservation for polarization transfer. Hence, if the ^{13}C–^{13}C dipolar interaction is recovered, facile transfer would occur. If

$$\Delta = \frac{|G_{11}|}{4} \tag{34}$$

is satisfied for a specific ^{13}C$_1$–^{1}H orientation, then the two ^{13}C spins resonate at δ_2. This leads to the modulation frequency for the ^{13}C–^{13}C dipolar Hamiltonian [Eq. (31)] being given by $m\nu_R$ ($m = \pm 1, \pm 2$). Noting that the time-dependent ^{13}C–^{1}H dipolar Hamiltonian oscillating at $n\nu_R$ ($n = 0,1,2,3$) remains in Eq. (25), we can express $\mathcal{H}_D^{IS*}(t) + \mathcal{H}_D^{SS*}(t)$ using a Fourier series as

$$\mathcal{H}_D^{IS*}(t) + \mathcal{H}_D^{SS*}(t) = \sum_{n=0,\pm 1,\pm 2,\pm 3} H_n \exp(2\pi i n \nu_R t). \tag{35}$$

We then adopt the secular average Hamiltonian approach [Eqs. (21)–(23)] to appreciate ^{13}C–^{13}C recoupling. For example, we have the following $n = 1$ term:

$$\mathcal{H}_{\pm 1} = -\frac{d_0}{8} g_{|1|}(S_{1+}S_{2-} + S_{1-}S_{2+})$$

$$+ \frac{G_{21}}{4} S_{1z}(I_z \mp iI_y)\exp(\pm 2i\gamma), \tag{36}$$

and the secular average Hamiltonian is obtained as

$$\mathcal{H}^{(1)} = \frac{d_0 g_{|1|} G_{21}}{64\pi\nu_R}(S_{1+}S_{2-} - S_{1-}S_{2+})\{(I_z - iI_y)$$

$$\times \exp(2i\gamma) - (I_z + iI_y)\exp(-2i\gamma)\}, \tag{37}$$

indicating that the ^{13}C–^{13}C dipolar interaction is recovered. This recoupling mechanism may be classified as resonant interference recoupling (RIR),[17] however, one should note that this RIR-based recoupling and DARR described in the previous section occur simultaneously at the rotary-resonance condition. To avoid confusion, we refer to this recoupling as second-order DARR and the case described in the Sec. B 1 as first-order DARR.

At first glance, one may consider recoupling efficiency is low in the second-order DARR, and is not appreciable. It is straightforward to show similar recoupling occurs between a pair of ^{13}C–^{1}H dipolar broadened resonances with spectral overlap as illustrated in Fig. 1(c). Such situation would occur for aliphatic carbons directly bonded to protons, and the

amount of spectral overlap is much larger than that of the first-order DARR [Fig. 1(a)]. We would also like to point out here that the ^{13}C CSA interaction neglected so far does also oscillate with $n\nu_R$ and thus interferes with the ^{13}C–^{13}C dipolar interaction, leading to ^{13}C–^{13}C recoupling for the pairs having degenerated resonance frequencies. This would enhance the efficiency of the second-order DARR recoupling among carbonyl and aromatic carbons. As will be shown experimentally afterward, these composite mechanisms do enhance the efficiency of the second-order DARR to be nearly comparable to that of the first-order DARR. The presence of the first- and second-order DARR mechanisms would make DARR to be broadband recoupling.

3. Resonant interference recoupling (RIR) by CW irradiation

To appreciate ^{13}C–^{13}C recoupling at off-rotary resonance conditions, we again rely on the secular average Hamiltonian theory instead of evaluating Eqs. (17) and (18) directly. In the present case, $\mathcal{H}_D^{IS*}(t)$ [Eq. (25)] oscillates with $\nu_1+n\nu_R$ ($n=\pm1,\pm2$), which causes a modulation-induced sidebands for the ^{13}C$_1$ spin (S_1). On the other hand, $\mathcal{H}_D^{SS*}(t)$ [Eq. (31)] oscillates with $\Delta+m\nu_R$ ($m=\pm1,\pm2$). Hence, RIR would occur in the case where the two modulation frequencies are matched with each other: the RIR conditions are given by

$$|\nu_1+n\nu_R|=|\Delta+m\nu_R|, \quad (n,m=\pm1,\pm2). \quad (38)$$

Let us consider the condition $\nu_R-\nu_1=\Delta-\nu_R$, at which one of the spinning sidebands of ^{13}C$_2$ is overlapped to one of the modulation-induced sidebands of ^{13}C$_1$ [Fig. 1(d)]. The latter sidebands are caused by the time-dependent ^{13}C–^{1}H dipolar interaction $\{(\mathcal{H}_D^{IS*}(t)$ [Eq. (25)]$\}$. Then we have

$$\mathcal{H}_D^{IS*}(t)+\mathcal{H}_D^{SS*}(t)=H_1\exp(2\pi i\nu_0 t)+H_{-1}$$
$$\times\exp(-2\pi i\nu_0 t) \quad (39)$$

with $\nu_0=\nu_R-\nu_1=\Delta-\nu_R$ and

$$H_{\pm1}=-\frac{g_1}{8}S_{1\pm}S_{2\mp}\exp(\mp i\gamma)+\frac{G_{11}}{4}(I_z\pm iI_y)S_{1z}$$
$$\times\exp(\pm i\gamma_1). \quad (40)$$

The first order secular average Hamiltonian is then obtained as

$$\mathcal{H}^{(1)}=-\frac{1}{2\pi(\Delta-\nu_R)}\left[\frac{g_1^2}{64}(S_{1z}-S_{2z})+\frac{G_{11}^2}{16}I_x\right.$$

$$+\frac{g_1 G_{11}}{32}\{S_{1+}S_{2-}(I_z-iI_y)\exp\{-i(\gamma+\gamma_1)\}$$

$$\left.+S_{1-}S_{2+}(I_z+iI_y)\exp\{i(\gamma+\gamma_1)\}\}\right]. \quad (41)$$

The $S_{1\pm}S_{2\mp}$ terms in Eq. (41) are relevant to ^{13}C–^{13}C polarization transfer.

C. ^{1}H-driven recoupling and "passive" DARR without ^{1}H irradiation

The spectral overlap discussed in Sec. II B 2 [Figs. 1(b) and 1(c)] may remind the conventional ^{1}H-driven mechanism, in which ^{13}C resonances are broadened by ^{13}C–^{1}H dipolar interactions under no rf irradiation and the spectral overlap occurs for a pair of ^{13}C spins with a chemical shift difference smaller than the broadening. It is therefore worthy to compare the two recoupling mechanisms under MAS, namely, the second-order DARR and the ^{1}H-driven recoupling. In both mechanisms, the spatial part of the ^{13}C–^{1}H dipolar interaction is modulated coherently by MAS. While in DARR the rf irradiation modulates the spin part coherently, in the ^{1}H-driven recoupling the modulation is *incoherent* because it is caused by the flip–flop transitions of the ^{1}H spins. For simplicity, we ignore the incoherency and simply assume the modulation frequency of the flip–flop motion to be ν_f. As shown in Eq. (16), the ^{13}C–^{13}C dipolar Hamiltonian $\mathcal{H}_D^{SS}(t)$ is modulated coherently by the chemical shift difference (Δ) and by MAS (ν_R). Hence, RIR would occur when $|\nu_f+m\nu_R|=|\Delta+n\nu_R|$. To phrase differently, in the ^{1}H-driven mechanism, the incoherent ^{1}H–^{1}H flip–flop motion serves as the coherent ^{1}H irradiation in RIR (Sec. II B 3). The ^{1}H-driven method is less efficient because the incoherent ^{1}H–^{1}H flip–flop modulation is less efficient as compared the coherent irradiation.

Digress for a moment to a related problem, we would like to point out here that ^{1}H rf irradiation can affect ^{1}H-driven polarization transfer in the following way. Kubo and McDowell derived the polarization transfer rate k under slow MAS for a pair of ^{13}C spins with a small chemical shift difference of Δ as[25]

$$k=\frac{\gamma_S^4 h^2}{15r^6}\sum_{n=1,2}\frac{M_n+M_{-n}}{n}\frac{T_R}{1+\Delta^2 T_R^2}, \quad (42)$$

where M_n is the intensity of the nth spinning sideband and T_R is the inverse of the linewidth of the zero-quantum line shape function, which is not known in most cases and thus commonly approximated by the apparent linewidth. Equation (42) indicates that the transfer rate reaches maximum at $\Delta T_R\sim1$, which suggests a possibility of enhancing the rate by choosing a proper ^{1}H rf strength to vary T_R and thus achieving $\Delta T_R\sim1$. In fact, we showed that there is an optimal ^{1}H rf strength for ^{13}C–^{13}C polarization transfer under slow MAS ($\nu_R=0.417-2.1$ kHz) among ^{13}CH$_3$ resonances ($\Delta\sim0.9$ ppm) of γ-valerolactone enantiomers enclathrated in the chiral cholic acid host.[26] Note that this mechanism is appreciable only at slow spinning and for a pair of spins with a small shift difference.

For a pair of ^{13}C spins with a chemical shift difference larger than the ^{13}C–^{1}H dipolar broadening, the ^{1}H-driven mechanism cannot work. However, we would like to point out that the spectral overlap due to line broadening caused by the time-dependent ^{13}C–^{1}H dipolar interaction under no ^{1}H irradiation would cause DARR around the R^2 condition ($\Delta\sim n\nu_R$). Since the ^{13}C–^{1}H dipolar broadening is homogenous, the most efficient spectral overlap would occur at the exact R^2 condition. In other words, the frequency-difference

TABLE I. ^{13}C$-^{13}$C recoupling mechanisms applicable for the two cases of chemical shift difference (Δ) with/without ^{13}C$-^1$H recoupling.

	no ^{1}H decoupling	^{13}C$-^1$H recoupling
Large Δ	passive DARR	first-order DARR
Small Δ	^{1}H-driven	second-order DARR

selectivity of the original R2 with ^{1}H decoupling is alleviated/deteriorated by the undecoupled ^{13}C$-^1$H dipolar interaction homogeneously modulated by the ^{1}H$-^1$H dipolar interaction. We refer to this as "passive" DARR, because the ^{13}C$-^1$H dipolar interaction is not recovered actively. It is worthy to note that for the "active" DARR no particular enhancement in recoupling efficiency is expected at the R^2 condition, because the amount of spectral overlap depends on the inhomogeneous ^{13}C$-^1$H dipolar powder line shape, which is not necessarily most efficient at the R^2 condition.

In Table I, we classify the first-order DARR, the passive DARR, the second-order DARR, and ^{1}H-driven according to the situations in which each of these recoupling methods is operative.

D. Efficiency of DARR and RIR

So far, we have shown that, under ^{1}H CW irradiation, efficient ^{13}C$-^{13}$C polarization transfer would occur at various recoupling conditions [Eqs. (33), (34), (38)], where the spectral overlap ensuring both energy conservation and recovery of the flip–flop term is achieved. Since these recoupling conditions include the chemical shift difference $\Delta = \delta_1 - \delta_2$, recoupling occurs frequency-difference selectively. Further, DARR is orientation selective due to G_{11} in Eqs. (33) and (34); recoupling takes place only for the ^{13}C$-^{13}$C pairs at particular orientations. It is therefore envisaged that polarization transfer by DARR is not efficient. As was shown by the previous DARR experiments with or without ^{1}H$-^1$H decoupling,[18] homogeneous broadening of the ^{13}C resonances due to nondecoupled ^{1}H$-^1$H interactions relaxes the recoupling condition, thus increasing the number of spins to be recoupled and also making DARR to be an efficient band-selective recoupling method. In addition to this, the second-order DARR mechanism would relax the selectivity, leading to broadband recoupling.

Since the orientation dependence of the recoupled ^{13}C$-^1$H dipolar powder pattern differs for different ^{13}C$-^1$H recoupling conditions, DARR can be improved by successive application of different ^{13}C$-^1$H recoupling conditions. In fact, it was shown that polarization-transfer efficiency is improved by alternating the ^{1}H rf-field strength between the two rotary-resonance conditions, $\nu_1 = \nu_R$ and $\nu_1 = 2\nu_R$, in a period of $\sim$0.5 ms.[18] For this purpose, MORE is more suitable because, while the rotary-resonance condition allows only two discrete ^{1}H rf-field strengths at a fixed MAS speed, MORE occurs irrespective to ^{1}H rf-field strength, thus allowing a larger number of a pair to participate in recoupling. This will be examined later.

For RIR [Eq. (38)], recoupling is achieved independent of the relative orientations of the interaction tensors involved. This means that most of ^{13}C$-^{13}$C pairs except for

that oriented along the magic angle participate in recoupling, thus increasing the net transfer efficiency. Due to the better spectral overlap, RIR is generally more efficient as compared to DARR. However, it should be noted that the magnitude of the RIR recoupling depends on the modulation frequency [Eq. (41)]. Hence, at fast modulation frequencies, RIR becomes less effective. Experimental comparison of RIR and DARR will be given below.

E. RIR by FSLG–$m\overline{2}\overline{m}m$

It should be pointed out that homogeneous broadening of the ^{13}C resonances due to ^{1}H$-^1$H couplings is not necessary for RIR or even becomes nuisance because it deteriorates the efficient spectral overlap. Hence, instead of the ^{1}H CW irradiation described so far, we adopt the FSLG-$m\overline{2}\overline{m}m$ ($m = 1$) sequence,[20] which modulates the ^{13}C$-^1$H dipolar interaction but decouples ^{1}H$-^1$H dipolar couplings by rf irradiation satisfying the Lee–Goldburg (LG) condition.[27] Under the FSLG-$m\overline{2}\overline{m}m$ sequence, the ^{13}C$-^1$H dipolar Hamiltonian is written as[20]

$$\mathcal{H}_D^{IS*}(t) = D_i(t)\cos\theta_M\{I_z\cos\theta_M + f(t)I_X\sin\theta_M\}S_{iz},$$
(43)

where $f(t)$ is a square-wave function. We expand $f(t)$ in the Fourier series and take accounts only of the first term,

$$f(t) \sim \frac{4}{\pi}\cos 2\pi\nu_{\text{Mod}}t,$$
(44)

where the modulation frequency ν_{Mod} is given by an inverse of the cyclic time τ_c of FSLG-$m\overline{2}\overline{m}m$ ($\nu_{\text{Mod}} = 1/\tau_c$). It is clear that the second term in Eq. (43) becomes time-independent at $\nu_{\text{Mod}} = n\nu_R (n = 1,2)$ (the ^{13}C$-^1$H recoupling condition).[20] Hence, FSLG-$m\overline{2}\overline{m}m$ can also be used to realize DARR, however, as was explained above and was shown experimentally,[18] DARR by FSLG-$m\overline{2}\overline{m}m$ is less effective due to the lack of homogeneous broadening.

At the modulation frequency deviated from the exact ^{13}C$-^1$H recoupling condition of $\nu_{\text{Mod}} = n\nu_R$, Eq. (43) can be given by[17]

$$\mathcal{H}_D^{IS*}(t) = \frac{2}{\pi}D_i(t)\cos(2\pi\nu_{\text{Mod}}t)\sin 2\theta_M I_x S_{iz}$$

$$= \frac{1}{2\pi}d_i\sum_{n=\pm1,\pm2}G_{in}\sin 2\theta_M\exp(in\gamma_i)$$

$$\times[\exp\{2\pi it(\nu_{\text{Mod}}+n\nu_R)\}$$

$$+ \exp\{-2\pi it(\nu_{\text{Mod}}-n\nu_R)\}]I_x S_{iz}.$$
(45)

The first I_zS_z term in Eq. (43) can be ignored, because it is averaged out by MAS. By comparing Eq. (25) and Eq. (45), we may rewrite the RIR condition under FSLG-$m\overline{2}\overline{m}m$ [Eq. (38)] as

$$|\nu_{\text{Mod}} + n\nu_R| = |\Delta + m\nu_R|, \quad (n,m = \pm1,\pm2).$$
(46)

For example, when ν_{Mod} is adjusted to satisfy $\nu_R - \nu_{\text{Mod}} = \Delta - \nu_R$, the first-order secular average Hamiltonian is given by[17]

$$\mathcal{H}^{(1)} = \frac{I_X}{\nu_R - \nu_{Mod}}(rS_{1+}S_{2-} + r^*S_{1-}S_{2+}), \qquad (47)$$

with

$$r = p(q_2 - q_1),$$

$$p = \frac{d_0}{8}g_1 \exp(-i\gamma),$$

and

$$q_n = \frac{\sin 2\theta_M}{2\pi}d_n G_{n1}\exp(-i\gamma_n). \qquad (48)$$

Since the recoupled Hamiltonian inversely depends on ν_R, RIR is less efficient at fast spinning as shown experimentally below.

III. EXPERIMENT

N-acetyl[1,2-^{13}C, ^{15}N] DL-valine ([1,2-^{13}C, ^{15}N] NAV) and uniformly ^{13}C, ^{15}N-labeled glycylisoleucine ([u-^{13}C, ^{15}N] GlyIle) were provided by Professor M. Kainosho at Tokyo Metropolitan University and his co-workers. [2,3-^{13}C] L-alanine ([2,3-^{13}C] Ala) was purchased from Cambridge Isotope Laboratories, Inc., and used without purification. A 10% [u-^{13}C, ^{15}N] GlyIle sample ($\sim$100 mg), obtained by recrystallization of [u-^{13}C, ^{15}N] GlyIle from deionized water with nine-fold natural abundance material, was used for two-dimensional (2D) ^{13}C–^{13}C polarization-transfer experiments.

The NMR experiments were carried out using a Chemagnetics CMX-300 spectrometer operating at the resonance frequency of 75.5 MHz for ^{13}C with a MAS probe (Doty Sci. Inc.) for a 5 mm rotor. The MAS frequency was kept constant within $\pm$10 Hz by a control system. The rf-field strength for cross polarization (CP) was about 53 kHz for ^{13}C and 63 kHz for ^{1}H. The ^{1}H CW decoupling frequency was chosen to be $\approx$2 ppm downfield from tetramethylsilane (TMS), and the ^{1}H rf-field strength for decoupling was $\approx$80 kHz.

For DARR, we examined three ^{13}C–^{1}H recoupling sequences: (1) rotary resonance recoupling[19] at the $n=1$ or $n=2$ rotary-resonance condition ($\nu_1 = n\nu_R$, $n=1,2$) [Fig. 2(a)], (2) modulatory resonance (MORE) recoupling[24] at the $n=1$ MORE condition ($\nu_{AM} = n\nu_R$, $n=1,2$), where $\nu_{AM} = 1/\tau_{AM}$ is the ^{1}H amplitude-modulation frequency [Figs. 2(b) and 2(c)], and (3) recoupling by rotor-synchronous π pulses applied at each half-rotor period [Fig. 2(d)], which was originally used for the rotational-echo double resonance (REDOR) experiment,[28] with a π-pulse duration time of 8.2 μs. In this work, the sinusoidal amplitude modulation originally employed for MORE [Fig. 2(b)] is approximated by a square-wave modulation achieved simply by phase alternation [Fig. 2(c)].

For RIR, we adopted the $m=2$ FSLG-$m\overline{2mm}$ sequence (FSLG–$2\overline{4}2$),[20] which consists of eight pulses with the same rf-field strength ν_1 and pulse duration time τ. The phase ϕ and the frequency offset δ for each pulse are given in order of $(\phi, \delta) = (X, \Delta\nu)$, $(-X, -\Delta\nu)$, $(-X, \Delta\nu)$, $(X, -\Delta\nu)$, $(-X, \Delta\nu)$, $(X, -\Delta\nu)$, $(X, \Delta\nu)$, and $(-X,$
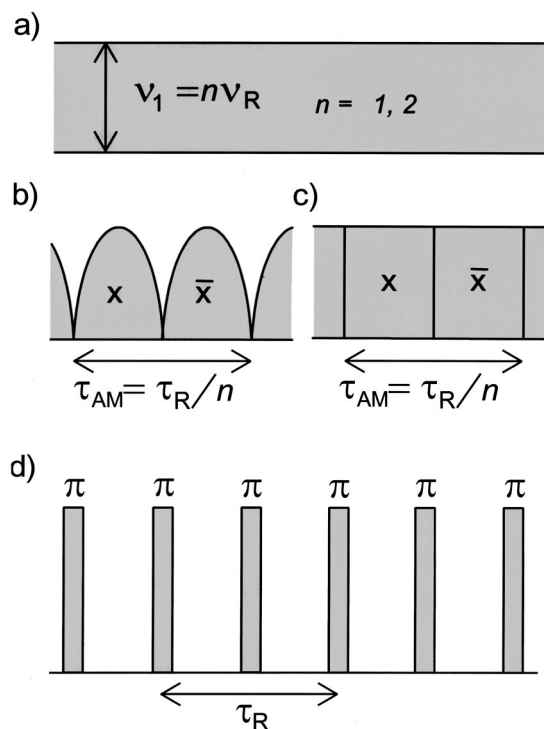

FIG. 2. Pulse sequences applied to ^{1}H for recoupling of the ^{13}C–^{1}H dipolar interaction under MAS. (a) CW irradiation at the rotational-resonance condition ($\nu_1 = n\nu_R$, $n=1,2$). (b) Irradiation with amplitude modulation at the MORE condition ($\tau_{AM} = \tau_R/n$, $n=1,2$), where τ_{AM} and τ_R are the cycle time of amplitude modulation and the rotation-period of MAS, respectively. (c) The sinusoidal modulation in (b) is approximated by a square-wave modulation for simplicity. (d) The rotor-synchronous π pulses applied at each half-rotation period.

$-\Delta\nu$). The offset and the rf strength for each pulse satisfy the Lee–Goldburg condition[27] of $\sqrt{2}\Delta\nu = \nu_1$ and the duration time is set to be the 2π nutation time around an effective field along the magic angle direction, $\tau = \sqrt{2/3}/\nu_1$. The rf intensity ν_1 required for fulfilling the RIR condition is given by Eq. (46) for given values of ν_R and Δ for a ^{13}C–^{13}C pair. For example, at $\nu_R = 12.0$ kHz and for $\Delta = 8.8$ kHz, the RIR condition of $\nu_{Mod} = \Delta$ [$n=m$ in Eq. (46)] is achieved when ν_1 was set to 62.0 kHz, which leads to the duration time for the 2π Lee–Goldburg pulse of 13.2 μs. Taking account of a 1 μs delay for switching the frequency and phase, we obtain the modulation frequency ν_{Mod} of 8.8 kHz. The ^{1}H mean frequency for the FSLG-$m\overline{2mm}$ sequence was 3000 Hz downfield from TMS.[20]

One-dimensional (1D) ^{13}C–^{13}C polarization-transfer experiments for [1,2-^{13}C, ^{15}N] NAV and [2,3-^{13}C] Ala were made as follows. The longitudinal ^{13}C magnetization is created by a 90° pulse after CP, and a selective-inversion soft pulse is applied to ^{13}C$_\alpha$ of [1,2-^{13}C, ^{15}N] NAV or [2,3-^{13}C] Ala. After a certain polarization-transfer time τ, the resulting longitudinal magnetization is observed by applying the second 90° pulse. During the polarization-transfer (mixing) time, one of the ^{13}C–^{1}H recoupling sequences described above is applied to ^{1}H. 2D ^{13}C–^{13}C polarization-transfer experiments of [u-^{13}C, ^{15}N] GlyIle were made by employing the conventional 2D exchange pulse sequence with DARR

achieved by the $n=1$ rotary-resonance ^{1}H irradiation during the mixing time.

IV. RESULTS AND DISCUSSION

In Sec. IV A, we examine ^{13}C–^{13}C polarization transfer between ^{13}C$=$O and ^{13}C$_\alpha$ in $[1,2$-^{13}C, ^{15}N$]$ NAV, in which the chemical shift difference is large (117 ppm–8.8 kHz at 7.0 T) and thus corresponds to the situations designated in Figs. 1(a) and 1(d). We show that three ^{13}C–^{1}H recoupling methods give similar DARR effects, and further compare ^{13}C–^{13}C polarization transfer efficiencies of the first-order DARR, the passive DARR, and RIR at various spinning rates. Effects of deviation from the exact ^{13}C–^{1}H recoupling condition on DARR are also examined. In Sec. IV B, we examine improvement of polarization-transfer efficiency of DARR by accumulating the number of the spins that participate in DARR. Polarization transfer by the second-order DARR and ^{1}H-driven recoupling is examined in Sec. IV C for ^{13}C$_\alpha$ and ^{13}CH$_3$ of $[2,3$-^{13}C$]$ Ala. Lastly in Sec. IV D, 2D ^{13}C–^{13}C polarization-transfer experiments on $[u$-^{13}C, ^{15}N$]$ GlyIle are reported in which DARR is applied during the polarization-transfer time (the mixing time). We show that the broadband nature of DARR is manifested at a long transfer time, which is useful for signal assignment and structure determination.

A. The first-order and passive DARR and RIR for large Δ

Figures 3(a) and 3(b) show ^{13}C CP/MAS spectra of $[1,2$-^{13}C, ^{15}N$]$ NAV at $\nu_R=12$ kHz with (a) and without ^{1}H CW decoupling (b). The ^{13}C$=$O and ^{13}C$_\alpha$ peaks appear at 4.4 and -4.4 kHz, respectively. Figures 3(c)–3(e) show spectra under ^{1}H rf irradiation at the $n=1$ rotary-resonance condition ($\nu_1=\nu_R$) (c), MORE with the ^{1}H rf-strength of $\nu_1\sim2\nu_R$ at the $n=1$ MORE condition ($\nu_{AM}=\nu_R$) (d), and the rotor-synchronized π pulses (e). The spectral overlap at a first spinning sideband of the ^{13}C$=$O peak, whose position is designated by the vertical dotted line, for the passive DARR is barely notable in Fig. 3(b), while those for the first-order DARR are prominent in Figs. 3(c)–3(e). These spectra [Figs. 3(c)–3(e)] also show that, under any recoupling condition, spectral overlap occurs between the ^{13}C–^{1}H dipolar powder pattern of ^{13}C$_\alpha$ and a first spinning sideband of ^{13}C$=$O. It is notable that the rotary resonance [Fig. 3(c)] and the π-pulse train [Fig. 3(e)] bring about appreciably larger ^{13}C–^{1}H dipolar broadening ($\sim\pm7$ kHz) than MORE ($\sim\pm5$ kHz) [Fig. 3(d)]. The results of the experimental investigation of this effect on DARR will be presented later.

1D DARR polarization-transfer NMR experiments were made by the four ^{1}H irradiation schemes corresponding to Figs. 3(b)–3(e). The observed polarization-transfer time dependence of the normalized difference magnetization $\langle M_{C=O}-M_{C\alpha}\rangle(\tau)/\langle M_{C=O}-M_{C\alpha}\rangle(0)$ in $[1,2$-^{13}C, ^{15}N$]$ NAV at $\nu_R=12$ kHz are shown in Fig. 4. It is noted that the ^{13}C–^{13}C polarization-transfer rates under the first-order DARR by the three ^{13}C–^{1}H recoupling sequences are comparable, and substantially faster than that under the passive DARR with no ^{1}H rf irradiation. Rotary resonance achieves
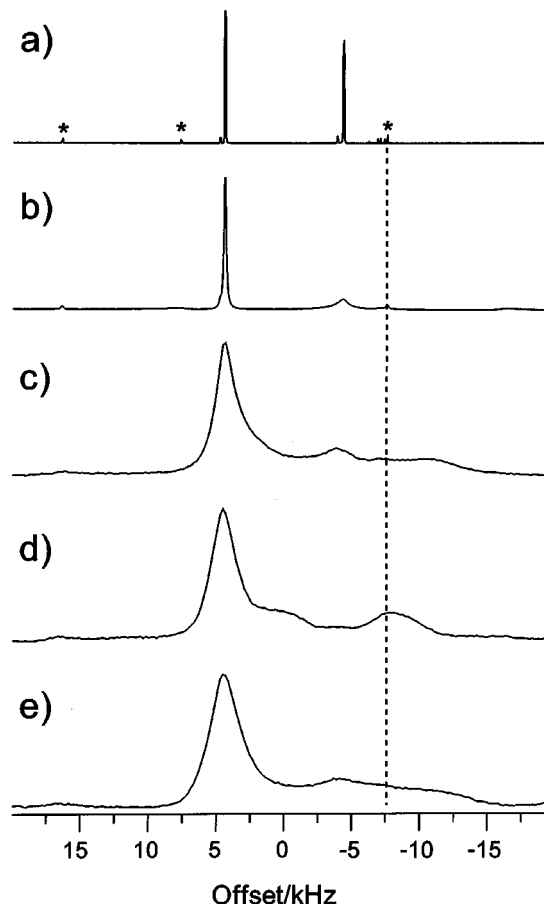

FIG. 3. ^{13}C CP/MAS spectra of N-acetyl$[1,2$-^{13}C, ^{15}N$]$ DL-valine at $\nu_R=12.0$ kHz: with ^{1}H CW decoupling (a), without ^{1}H decoupling (b), with ^{1}H rf irradiation for ^{13}C–^{1}H recoupling by $n=1$ rotary resonance ($\nu_1=\nu_R$) (c) and with the ^{1}H rf-strength of $\nu_1\sim2\nu_R$ at the $n=1$ MORE condition ($\nu_{AM}=\nu_R$) (d), and with the rotor-synchronized π pulses (e). The peaks marked by asterisks are spinning sidebands, and other small peaks are due to naturally abundant ^{13}C peaks. The vertical dotted line shows the position of a first spinning sideband of the ^{13}C$=$O peak.

the largest amount of polarization transfer among the three ^{13}C–^{1}H recoupling schemes. This may be ascribed to the absence of phase transients and finite pulse rise times in the ^{1}H rf sequence.

The region as well as the amount of spectral overlap should be different at different spinning speeds. Hence, it is expected that the polarization transfer rate depends on ν_R. The Hamiltonian recoupled by RIR in particular does depend on ν_R [Eq. (47)]. Therefore, it is interesting to examine 1D ^{13}C–^{13}C polarization-transfer rates at various ν_R. The apparent polarization-transfer rates k were deduced by fitting the initial decay ($\leqslant2$ ms) of the polarization-transfer curves for ^{13}C$=$O and ^{13}C$_\alpha$ in $[1,2$-^{13}C, ^{15}N$]$ NAV (similar to those in Fig. 3, not shown) to a single exponential function $\exp(-k\tau)$. At least 6 data points were observed for each curve and used for fitting. The obtained k values are plotted in Fig. 5 for experiments with the first-order DARR at the $n=1$ and $n=2$ rotary-resonance conditions, the passive DARR, and RIR under FSLG-2$\bar{4}$2 at the RIR condition of $|\nu_{Mod}+\nu_R|=|\Delta+2\nu_R|$.

In Fig. 5, the fastest rate observed is that for the passive DARR at the rotational-resonance (R^2) condition $\Delta=\nu_R$
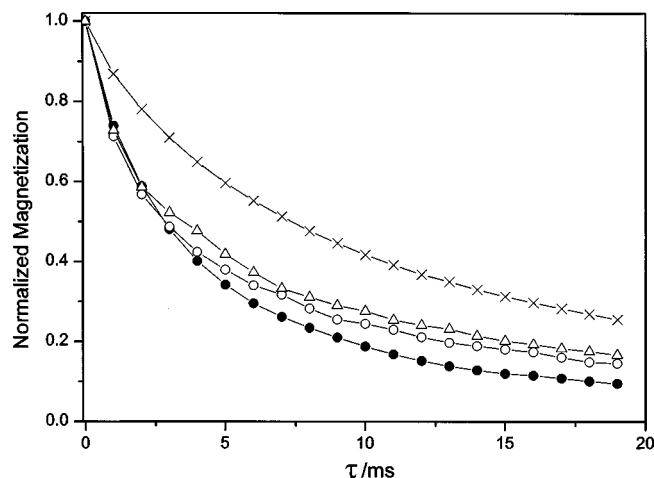
FIG. 4. Polarization-transfer time dependence of the normalized difference magnetization, $\langle M_{C=O} - M_{C\alpha}\rangle(\tau)/\langle M_{C=O} - M_{C\alpha}\rangle(0)$ for $^{13}C=O$ and $^{13}C_\alpha$ in N-acetyl[1,2-^{13}C, ^{15}N] DL-valine at $\nu_R = 12$ kHz. The $^{13}C_\alpha$ magnetization is selectively inverted before the polarization-transfer time. Four different ^{1}H rf irradiation schemes during the polarization-transfer time were examined: (1) no rf irradiation ($\times$), (2) irradiation with the $n=1$ rotary-resonance condition ($\bullet$), (3) phase-alternated rf irradiation (MORE) with the ^{1}H rf-strength of $\nu_1 \sim 2\nu_R$ at the $n=1$ MORE condition ($\nu_{AM} = \nu_R$) ($\bigcirc$), and (4) the rotor-synchronized π pulses ($\triangle$). The lines are drawn for eye guidance.

$= 8.8$ kHz. It is also shown that the rate under the passive DARR depends appreciably on the spinning speed, and the rate becomes slow at faster spinning. On the other hand, it is clear that no particular enhancement of transfer occurs at the R^2 condition for the first-order DARR and RIR experiments. This relaxes the experimental choice of ν_R for a $^{13}C-^{13}C$ DARR/RIR polarization-transfer experiment for a multiply ^{13}C-labeled sample. Figure 5 also shows that the first-order

FIG. 6. ^{13}C CP/MAS spectrum of N-acetyl[1,2-^{13}C, ^{15}N] DL-valine at $\nu_R = 15$ kHz under ^{1}H rf irradiation of (a) DARR with the $n=2$ rotary-resonance condition ($\nu_1 = 30$ kHz) and (b) DARR with an "off" rotary-resonance condition of $\nu_1 = 35$ kHz, at which the polarization-transfer rate reaches one of the local maxima (Fig. 7). The vertical dotted line shows the position of a first spinning sideband of the $^{13}C=O$ peak.

FIG. 5. Dependence of the polarization-transfer rate (k) between $^{13}C=O$ and $^{13}C_\alpha$ in N-acetyl[1,2-^{13}C, ^{15}N] DL-valine on the MAS speed ν_R under various recoupling schemes: (1) ^{1}H-driven with no rf irradiation ($\times$), (2) DARR by the $n=1$ rotary-resonance irradiation ($\bullet$), (3) DARR by the $n=2$ rotary-resonance irradiation ($\triangledown$), (4) DARR by the $n=1$ MORE irradiation with the ^{1}H rf-strength of $\nu_1 \sim 2\nu_R$ ($\bigcirc$), and (5) RIR by FSLG-2$\bar{4}$2 ($\square$). The rates were deduced by fitting the initial decay in the polarization-transfer curves for the difference of the magnetizations of the two carbons to a single exponential function $\exp(-k\tau)$. The lines are drawn for eye guidance.
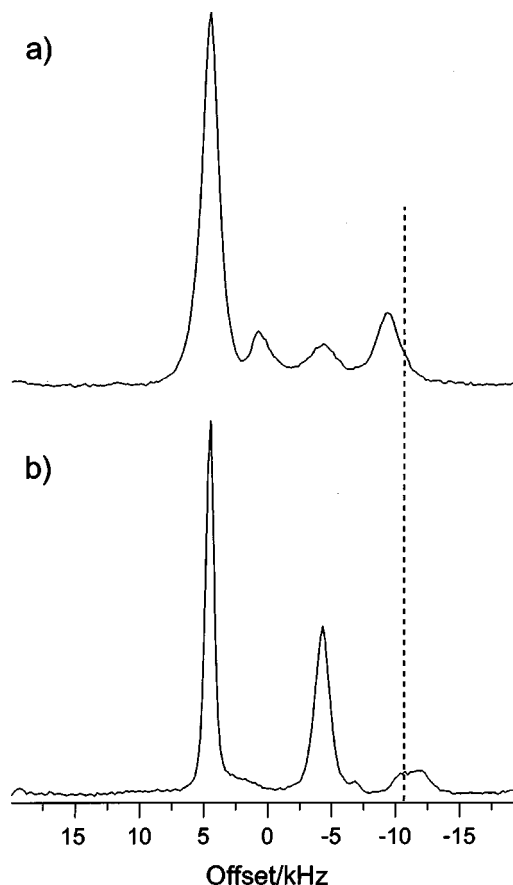
DARR is less efficient as compared to RIR for a spinning speed below 13 kHz. The inefficiency of DARR compared to RIR is ascribed to the orientation dependence of the DARR condition, that is, not all ^{13}C spin pairs participate in DARR. However, as expected from Eq. (47), the transfer rate under RIR becomes lower for faster speeds and comparable to that under DARR at $\nu_R \sim 14$ kHz. It is further noted that at higher spinning, DARR by the $n=2$ rotary-resonance irradiation becomes less efficient. Figure 6(a) shows the ^{13}C CP/MAS spectrum observed for [1,2-^{13}C, ^{15}N] NAV under ^{1}H rf irradiation with the $n=2$ rotary-resonance condition at $\nu_R = 15$ kHz, indicating that the broadening at the $n=2$ condition is smaller ($\sim \pm 5$ kHz) than that at the $n=1$ condition. Figure 6(a) also shows that the slow rate for the $n=2$ condition at $\nu_R \geq 14$ kHz (Fig. 5) is attributed to inadequate spectral overlap because the MAS speed exceeds the sum of the chemical-shift difference (8.8 kHz) and the dipolar broadening (~ 5 kHz). Among the four experiments, we found that DARR at the $n=1$ rotary-resonance condition is the most insensitive to the spinning speed ν_R. This is ascribed to the large $^{13}C-^1$H dipolar broadening (~ 7 kHz) under the $n=1$ rotary-resonance recoupling [Fig. 3(c)], which provides almost constant amounts of spectral overlap
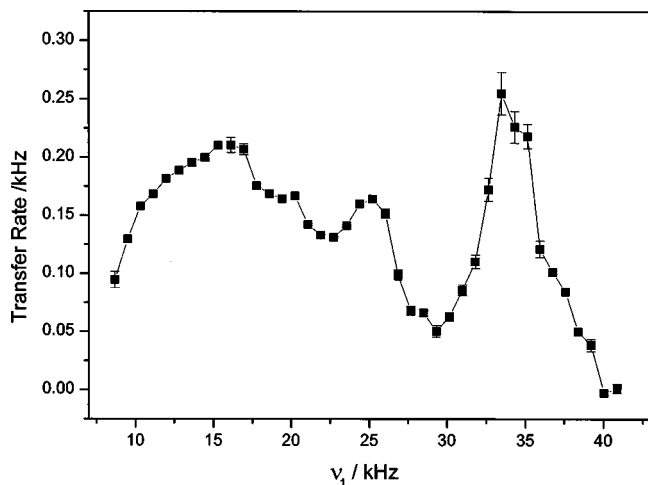
FIG. 7. Dependence of the polarization-transfer rate (k) between ^{13}C=O and ^{13}C$_\alpha$ of N-acetyl[1,2-^{13}C, ^{15}N] DL-valine on the ^{1}H rf-field intensity ν_1 at $\nu_R=15$ kHz. The procedure to deduce the rates is described in the caption of Fig. 5. The line is drawn for eye guidance.
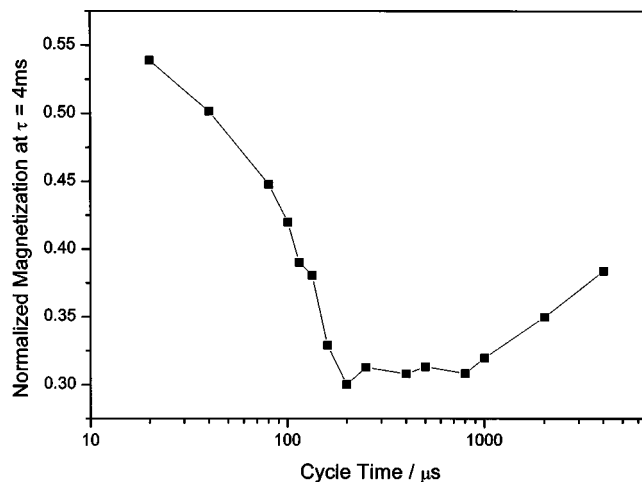

FIG. 8. Alternation-interval dependence of the normalized difference magnetization in the 1D DARRAM polarization-transfer experiment with the transfer time of 4 ms at $\nu_R=12$ kHz. The difference was taken for ^{13}C=O and ^{13}C$_\alpha$ of N-acetyl[1,2-^{13}C, ^{15}N] DL-valine. The line is drawn for eye-guidance.

for the MAS speed examined.

The results examined so far indicate that it is not necessary to optimize the ^{13}C–^{1}H recoupling for increasing efficiency of the ^{13}C–^{13}C transfer as long as line broadening necessary for spectral overlap is achieved. To show this more explicitly, 1D ^{13}C–^{13}C polarization-transfer NMR experiments under ^{1}H CW irradiation at various rf strengths (ν_1) were done at $\nu_R=15$ kHz, and the observed initial transfer rates k are plotted in Fig. 7. One broad maximum is found at the $n=1$ rotary-resonance condition ($\nu_1=\nu_R=15$ kHz), which is attributed to the first-order DARR, and two other maxima at 25 and 35 kHz are deviated by $\sim\pm5$ kHz from the $n=2$ rotary-resonance condition ($\nu_1=2\nu_R=30$ kHz). The broad maximum around the $n=1$ rotary-resonance condition indicates that slight misadjustment of the ^{1}H rf intensity or the spinning frequency is not crucial for the first-order DARR by the $n=1$ rotational-resonance irradiation. The observed tolerance would alleviate precise settings of experimental conditions often required for the rf-driven ^{13}C–^{13}C recoupling experiments. On the other hand, the $n=2$ rotary-resonance condition is not a good choice for DARR: the optimal irradiation condition deviates significantly from the exact DARR condition (Fig. 7). This can be attributed to the particular ^{13}C–^{1}H dipolar broadening line shape of the ^{13}C$_\alpha$ carbon of [1,2-^{13}C, ^{15}N] NAV as follows. Figure 6(b) shows the ^{13}C CP/MAS spectrum of [1,2-^{13}C, ^{15}N] NAV under ^{1}H rf irradiation at $\nu_1=35$ kHz and $\nu_R=15$ kHz, at which k reaches one of the two local maxima (Fig. 7). The spectrum shows characteristic three ridge peaks and the fast transfer at $\nu_1=35$ kHz evidently arises from the spectral overlap at one of the ridges of the ^{13}C$_\alpha$ resonance and a first spinning sideband of the ^{13}C=O peak, whose position is indicated by the dotted line. It should be noted here that the recoupling mechanism in this case is not DARR but RIR, and the presence of the RIR mechanism also helps to broaden the maximum around the $n=1$ condition (Fig. 7).

B. Improvement of DARR

As shown above, the amount of spectral overlap should be as large as possible for efficient ^{13}C–^{13}C polarization transfer under DARR. This was also shown by a previously reported experimental result that polarization transfer under DARR by the rotary-resonance irradiation is appreciably faster than that by the FSLG-$m\overline{2}\overline{m}m$ ^{13}C–^{1}H recoupling sequence.[18] The homogeneous broadening of ^{13}C resonances due to the nonzero ^{1}H–^{1}H interaction under rotary resonance increases the number of carbons to be recoupled, leading to faster transfer. Further, we showed that ^{13}C–^{13}C polarization-transfer efficiency can be improved by alternating the ^{1}H rf-field strength between the $n=1$ and $n=2$ rotary-resonance conditions in a period of 0.25 ms.[18] This was also ascribed to the increase of the number of ^{13}C spins satisfying the DARR condition. The scheme was referred to as DARR with alternate matching (DARRAM). To examine how long the alternation interval should be, we observed 1D polarization transfer for ^{13}C=O and ^{13}C$_\alpha$ in [1,2-^{13}C, ^{15}N] NAV with several alternation periods for DARRAM at $\nu_R=12$ kHz, and the normalized difference magnetization at the polarization-transfer time of 4 ms, $\langle M_{C=O}-M_{C\alpha}\rangle(\tau=4\text{ ms})/\langle M_{C=O}-M_{C\alpha}\rangle(0)$, is plotted as a function of alternation interval in Fig. 8. Note that the alternation interval of 4 ms (the data at the extreme right in Fig. 8) corresponds to DARR without alternation. Transfer efficiency is improved evidently for the interval of 200–800 μs. This is reasonable because the ^{13}C–^{13}C dipolar interaction is in the order of a few kHz in [1,2-^{13}C, ^{15}N] NAV, thus accumulative transfer would occur in a time scale of a few 100 μs. For a weaker ^{13}C–^{13}C dipolar interaction, a longer alternation time is required.

Improvement of ^{13}C–^{13}C transfer by accumulating the number of ^{13}C spins participating in transfer can be most easily accomplished for MORE by simply optimizing ^{1}H rf-strength because of the unique feature that the ^{13}C–^{1}H recoupling condition does not depend on ^{1}H rf-field strength,
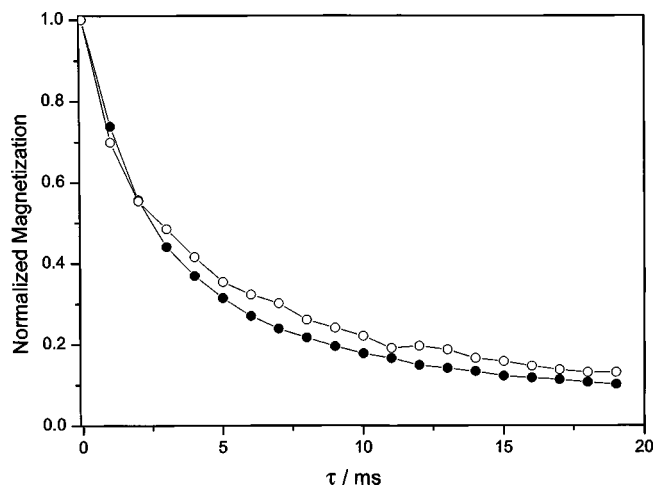
FIG. 9. Polarization-transfer-time dependence of the normalized difference magnetization of $^{13}C=O$ and $^{13}C_\alpha$ in N-acetyl[1,2-^{13}C, ^{15}N] DL-valine in the 1D polarization transfer-experiment under DARR with MORE ($\bigcirc$) and variable-amplitude MORE ($\bullet$) at $\nu_R = 12$ kHz. The lines are drawn for eye-guidance.

but the recoupled line shape does.[24] In fact, the ^{1}H rf-field strength of $\nu_1 \sim 2\nu_R$ in Fig. 3(d) was chosen to maximize apparent spectral overlap for the two ^{13}C line shapes at $\nu_R = 12$ kHz. For a $^{13}C-^{13}C$ transfer experiment under DARR by variable-amplitude MORE, the ^{1}H rf-field strength was varied linearly from $0.5\nu_R$ to $2.5\nu_R$ with the cycle time of 2.5 ms divided into 10 segments during each of which the ^{1}H rf intensity was kept constant. In Fig. 9, we compare the observed transfer curve with that observed with constant-amplitude MORE [Fig. 2(c)]. Figure 9 shows that DARR efficiency is improved by sweeping over the whole region of the $^{13}C-^1$H dipolar powder pattern.

The improved irradiation schemes for DARR increase not only the total amount of polarization transfer but also the apparent transfer rate. We would like to point out that the improved efficiency should be useful for reduction of a time required to achieve uniform signal enhancement by the nuclear Overhauser polarization (NOP).[21]

C. The second-order DARR and ^{1}H-driven recoupling for small Δ

Figures 10(a) and 10(b) show ^{13}C CP/MAS spectra of [2,3-^{13}C] Ala at $\nu_R = 12$ kHz with (a) and without ^{1}H CW decoupling (b), in which the $^{13}CH_3$ and $^{13}C_\alpha$ peaks appear at -2.3 and 0 kHz, respectively. Figures 10(c) and 10(d) show the spectra observed under $^{13}C-^1$H recoupling using the $n = 1$ rotary-resonance irradiation and under ^{1}H rf irradiation at "off" rotary resonance of $\nu_1 = 29$ kHz, respectively. Figures 10(b) and 10(c) show that spectral overlap suitable for the second-order DARR [Fig. 10(c)] is appreciably improved as compared to that by ^{1}H-driven recoupling [Fig. 10(b)]. This better overlap leads to the polarization-transfer-rates by the second-order DARR which are $\sim$1.6–1.8 times as fast as those by ^{1}H-driven recoupling at the most of the spinning rates examined (Fig. 11). The dotted line in Fig. 11 represents $k(\text{kHz}) = 3.0/\nu_R(\text{kHz}) - 0.14$, showing the $1/\nu_R$ dependence predicted in Eq. (37), where the coefficients in the
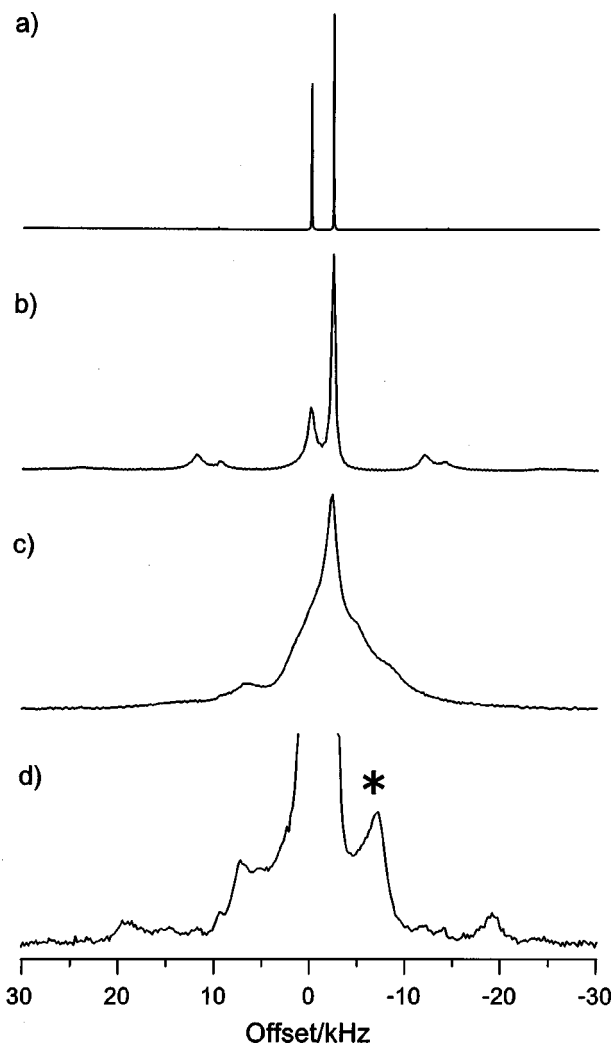

FIG. 10. ^{13}C CP/MAS spectra of [2,3-^{13}C] L-alanine at $\nu_R = 12$ kHz with ^{1}H CW decoupling (a), without ^{1}H decoupling (b), with ^{1}H rf irradiation by $n = 1$ rotary resonance ($\nu_1 = \nu_R$) (c), and by "off" rotary resonance with $\nu_1 = 29$ kHz (d). The asterisk denotes a ridge peak of the $^{13}C_\alpha$ resonance. The ridgepeak frequency depends on ν_1 as shown in Fig. 13.

equation were obtained by curve fitting. The enhanced polarization transfer and the $1/\nu_R$ dependence prove that the polarization transfer is due to the second-order DARR recoupling. Figure 12 shows the ν_1 dependence of the transfer rate in DARR at $\nu_R = 12$ kHz. The rate is almost constant for $\nu_1 = 5$–23 kHz, and two local maxima appear at $\nu_1 = 31.5$ and 37 kHz. The apparent insensitivity to ν_1 below 23 kHz together with the similar results for the first-order DARR shown in Fig. 7 indicate that the $n = 1$ rotary-resonance condition is a good choice for $^{13}C-^{13}C$ transfer with DARR.

The two local maxima at $\nu_1 \sim 31$ and ~ 37 kHz can be ascribed to the particular $^{13}C-^1$H dipolar broadened line shape of the $^{13}C_\alpha$ carbon in [2,3-^{13}C] Ala at off-rotary resonance conditions [Fig. 10(d)]. Figure 13 shows the ν_1 dependence of the shift of a specific ridge peak of the $^{13}C_\alpha$ resonance denoted by an asterisk in Fig. 10(d). The shift increases with increasing ν_1, and at $\nu_1 \sim 37$ kHz the ridge peak overlaps with a first spinning sideband of the $^{13}CH_3$ peak, whose shift position is indicated by the dotted line in Fig. 13, leading to the local maximum. The other local maxi-
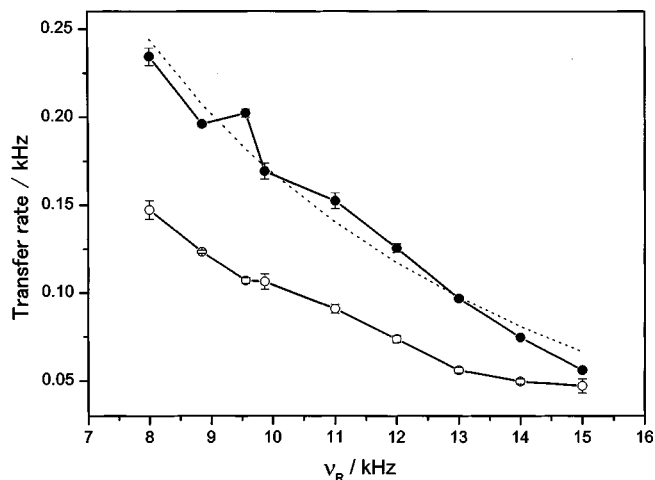
FIG. 11. Dependence of the polarization-transfer rate (k) for ^{13}C$_\alpha$ and ^{13}C=O in [2,3-^{13}C] L-alanine on the MAS speed ν_R under (1) no rf irradiation (○) and (2) rf irradiation with the $n=1$ rotary-resonance condition (●). The procedure to deduce the rates is described in the caption of Fig. 5. The dotted line, $k(\text{kHz})=3.0/\nu_R(\text{kHz})-0.14$, shows the $1/\nu_R$ dependence indicated in Eq. (37) for the second-order DARR. The solid lines are drawn for eye guidance.

FIG. 13. Offset-frequency dependence of the ^{13}C$_\alpha$ ridge peak marked by an asterisk in Fig. 10(d) on the ^{1}H rf irradiation strength ν_1. The horizontal dotted line indicates the position of a first spinning sideband of the CH$_3$ peak. The solid line is for eye guidance.

mum at 31 kHz can also be ascribed to the overlap of a ridge peak of the ^{13}CH$_3$ resonance and a sideband of the ^{13}C$_\alpha$ peak.

    We would like to point out here that the observed transfer rates of 0.1–0.2 kHz by the second-order DARR are almost comparable to those (Fig. 5) by the first-order DARR ($k\sim 0.2$–0.4 kHz). Even though the recoupling occurs in the second-order, a large amount of spectral overlap for the second-order DARR may improve recoupling efficiency to be comparable to that of the first-order DARR.

D. Broadband ^{13}C–^{13}C polarization-transfer experiments using DARR

    Since no ^{13}C rf field is required for ^{13}C–^{1}H dipolar-driven recoupling, the polarization-transfer time is only lim-
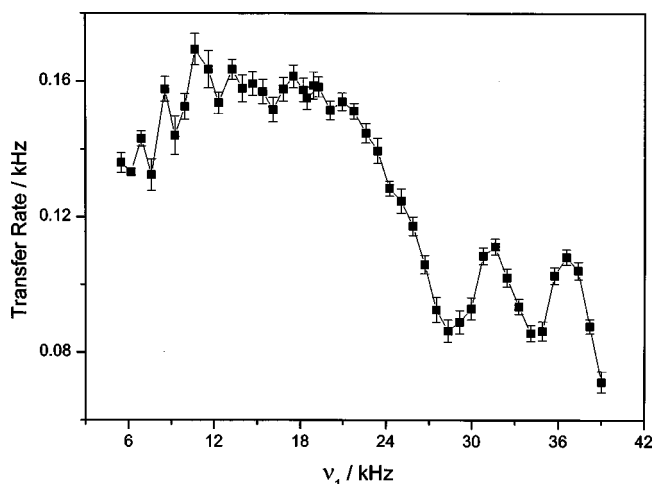

FIG. 12. Dependence of the polarization-transfer rate (k) for ^{13}C$_\alpha$ and ^{13}C=O in [2,3-^{13}C] L-alanine on the ^{1}H rf-field intensity ν_1 at $\nu_R=12$ kHz. The procedure to deduce the rates is described in the caption of Fig. 5. The line is drawn for eye guidance.
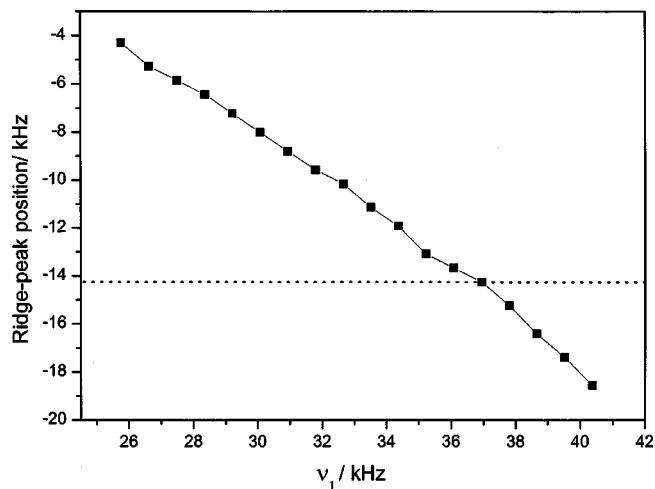
ited by long ^{13}C spin-lattice relaxation. Therefore, even if the recoupled dipolar Hamiltonian by ^{13}C–^{1}H dipolar-driven recoupling is smaller than those recoupled by the rf-driven methods, the interspin distances which can be correlated by ^{13}C–^{13}C transfer using ^{13}C–^{1}H dipolar-driven recoupling may be comparable to or even longer than those by the rf-driven methods. While the first-order DARR and RIR show band-selective nature useful for recoupling sp^2 carbons and sp^3 carbons, the second-order DARR is applicable to recouple sp^2 or sp^3 carbons. Hence, DARR would achieve a broadband recoupling nature. To examine this, we performed 2D ^{13}C–^{13}C polarization-transfer experiments with DARR applied during the mixing time.

    Figure 14 shows 2D ^{13}C–^{13}C polarization-transfer spectra observed for 10% [u-^{13}C, ^{15}N] GlyIle at the spinning frequency $\nu_R=15.0$ kHz with the polarization-transfer time of 10 ms (a) and 200 ms (b) together with the individual cross-section spectra at the carbonyl carbon resonance (~ 178.9 ppm) (Ref. 29) of the isoleucine residue (C$^{\text{Ile}}$=O). DARR is achieved by applying ^{1}H rf irradiation at the $n=1$ rotary-resonance condition. A similar 2D DARR experiment with the transfer time of 3 ms has been done using 100% [u-^{13}C, ^{15}N] GlyIle to show that the first-order DARR with a short transfer time exhibits only the cross peaks between directly bonded C=O and C$_\alpha$.[18] At the transfer time of 10 ms, however, all the cross peaks expected for the directly bonded carbon pairs are observed owing to the second-order DARR recoupling. Hence, the DARR correlation experiment is useful for signal assignment. Further at 200 ms, cross peaks between carbons separated by several bonds are observed in addition to the direct bonded carbons. For example, let us examine the cross-section spectrum at C$^{\text{Ile}}$=O. The intensities of the individual cross peaks in the C$^{\text{Ile}}$=O cross-section spectrum, which are obtained by fitting a sum of Lorenzian lineshapes to the cross section, are normalized by the peak intensity of C$^{\text{Ile}}$=O and plotted in Fig. 15 against the corresponding C–C distances calculated from the atomic coordinates determined by an x-ray diffraction study

a)   b)
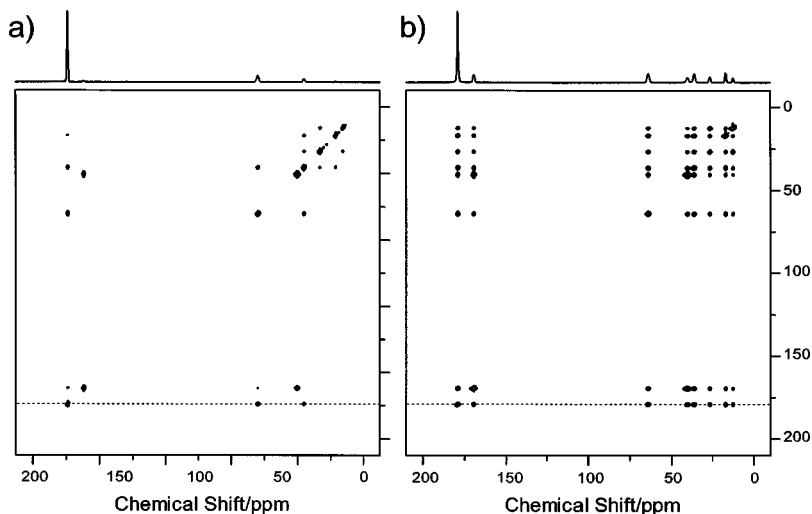

FIG. 14. Contour plots of 2D ^{13}C–^{13}C polarization-transfer spectra of 10% uniformly ^{13}C, ^{15}N-labeled gly-cylisoleucine with the polarization-transfer time of 10 ms (a) and 200 ms (b). The top spectrum is the cross section at the carbonyl carbon resonance ($\sim$178.9 ppm) of the isoleucine residue (C^{Ile}═O). The dotted line is drawn at the position of C^{Ile}═O. During the polarization-transfer time, ^{1}H rf irradiation to enhance ^{13}C–^{13}C polarization transfer by DARR with the $n=1$ rotary resonance was applied. The spinning frequency was 15.0 kHz.

(unpublished). Figure 15 clearly shows that the cross-peak intensity and the internuclear distance are well correlated with each other. Similar correlation has also been observed in the nuclear Overhauser polarization (NOP) experiments using DARR.[21] In analyzing ^{13}C–^{13}C transfer from methyl carbons to the other carbons in [u-^{13}C, ^{15}N] GlyIle, we found that the polarization-transfer rate from the polarized $^{13}CH_3$ spin to the other ^{13}C spin correlates well with the ^{13}C–^{13}C distance.

It has been pointed out that recoupling of a strong ^{13}C–^{13}C dipolar interaction suppresses recoupling of weak ones between a ^{13}C spin of the strong dipolar pair and remote ^{13}C spins.[30–32] This dipolar truncation would make it difficult to observe long-range correlation, while it appears that the dipolar truncation effect is less appreciable for DARR. The suppression of the dipolar truncation effect may be ascribed to the orientation-selective recoupling of DARR. Since DARR recouples a pair of spins with a particular orientation,
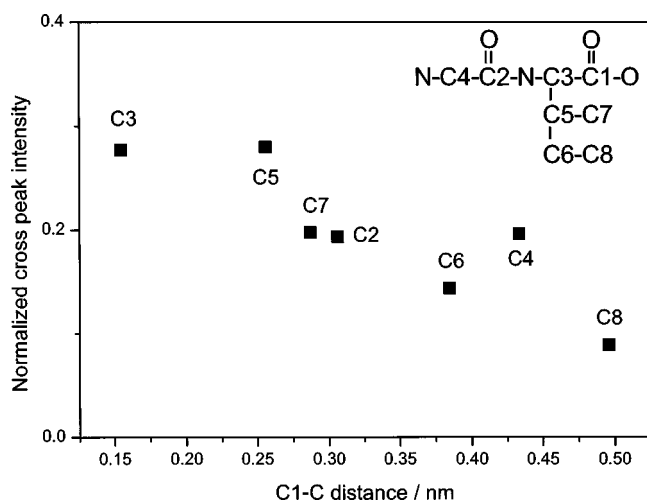
not all ^{13}C–^{13}C couplings in a molecule are recovered at the same time. Hence, the uniformly labeled spins are partitioned into fragments of recoupled spins, leading to isolation of a weak coupling. In other words, while the sample is uniformly ^{13}C-labeled, DARR recoupling does not occur uniformly. This unique feature of DARR causes us to have the expectation that many distances restrains can simultaneously be obtained from cross-peak intensities in a 2D DARR spectrum. However, the intensity is affected by several factors, such as the amount of spectral overlap, different efficiencies of the first-order and the second-order DARR, effects of CSA on sideband intensities, and homogeneous broadening due to ^{1}H–^{1}H dipolar interactions, making the explanation of the cross-peak intensity difficult. Nevertheless, we found that the polarization-transfer rate correlates well with the internuclear distance. This empirical correlation indicates a possibility of determining complete structures of biological systems by the polarization transfer experiment under DARR. To examine the correlation in more detail, we are currently measuring build-up rates of individual cross-peak intensities in several uniformly ^{13}C-labeled peptides with known structures.

V. CONCLUDING REMARKS

In this work, using the average Hamiltonian theory, we examined two recently introduced ^{13}C–^{1}H dipolar-driven ^{13}C–^{13}C recoupling methods under MAS: dipolar assisted rotational resonance (DARR) and resonant interference recoupling (RIR). In both methods, rf irradiation for recoupling is applied only to ^{1}H spins, and spectral overlap for a ^{13}C–^{13}C pair is achieved between a spinning sideband of one ^{13}C spin and the ^{13}C–^{1}H dipolar pattern of the other ^{13}C spin. Then, ^{13}C–^{13}C recoupling based on rotational resonance (R^2) occurs frequency-difference selectively.

In DARR, we recover time-independent ^{13}C–^{1}H dipolar interactions by a suitable ^{13}C–^{1}H recoupling method, and then the spectral overlap occurs for a pair of spins with a particular internuclear orientation. Thus, DARR causes orientation-selective recoupling. On the other hand, in RIR, ^{13}C–^{1}H dipolar interactions are modulated both by MAS and by ^{1}H rf irradiation: a ^{1}H rf-field is applied to modulate the

FIG. 15. Correlation between the normalized cross-peak intensity obtained from the 2D ^{13}C–^{13}C polarization-transfer spectrum of 10% uniformly ^{13}C, ^{15}N-labeled glycylisoleucine with the polarization-transfer time of 200 ms [Fig. 14 (b)] and the C–C distance to the C^{Ile}═O carbon (C1) for C2–8 in 10% uniformly ^{13}C, ^{15}N-labeled glycylisoleucine together with a schematic molecular structure. The carbon numbering starts from ^{13}C resonances at the higher-frequency side.

^{13}C–^{1}H dipolar interaction in such a way to interfere with the ^{13}C–^{13}C dipolar interaction. Since RIR relies on spectral overlap between a CSA spinning sideband of one ^{13}C peak of the pair and a modulation-induced ^{13}C–^{1}H dipolar sideband of the other ^{13}C peak, the RIR recoupling condition does not involve any internuclear orientation. Hence, the number of spins participates in recoupling is much larger for RIR than for DARR, which may lead RIR to a more efficient ^{13}C–^{13}C polarization transfer method. In fact, we found that RIR is more efficient than DARR at slow spinning, but its efficiency depends on a spinning speed [Eq. (47)] and thus decreases appreciably at a faster spinning speed.

We showed that ^{1}H CW irradiation under rotary-resonance conditions induces recoupling due to DARR and RIR at various matching conditions [Eqs. (33), (34), (38)]. In particular, we showed that the second-order DARR recoupling [Eq. (34)] occurs for a pair of spins whose chemical shift difference is too small to achieve the first-order DARR condition [Eq. (33)]. This makes it possible to realize a broadband 2D ^{13}C–^{13}C correlation experiment by DARR. In fact, we showed by the 2D ^{13}C–^{13}C DARR polarization-transfer experiment of [u-^{13}C, ^{15}N] GlyIle that broadband correlation in a multiple spin system is achieved by DARR.

Not only rotary resonance, but also MORE and rotor-synchronized π pulses were examined for ^{13}C–^{1}H recoupling schemes in DARR. We found that the $n=1$ rotary resonance is the most suitable for DARR, because of the observed insensitivity to experimental settings of a ^{1}H rf-field strength and a spinning speed, and the broad recoupling bandwidth. Further, we showed that ^{13}C–^{13}C polarization-transfer efficiency can be improved by a combined use of more than one ^{13}C–^{1}H recoupling condition, which increases the number of spins participating in recoupling.

It was suggested that the suppression of recoupling of weaker dipolar couplings by stronger ones (the dipolar truncation) becomes less prominent due to the orientation selectivity of DARR. This unique feature may make DARR as a possible tool of determining internuclear distances roughly by the polarization transfer experiment. In fact, the 2D DARR polarization-transfer experiment of [u-^{13}C, ^{15}N] Gly-Ile in this work and the NOP experiment using DARR (Ref. 21) show that the polarization-transfer rate for a ^{13}C–^{13}C pair correlates well with the internuclear distance of the ^{13}C–^{13}C pair. Hence, a 2D DARR polarization-transfer experiment may be applied to obtain structural information of a multiply ^{13}C-labeled sample. For example, a preliminary 2D DARR polarization-transfer experiment of a peptide Lys-Phe*-Ile*-Gly*-Leu*-Met (* denotes a fully ^{13}C labeled amino acid residue) has revealed a pair of inter-residue cross peaks between ^{13}C$_{\alpha}$ of Phe and ^{13}C$_{\beta}$ of Leu at the transfer time ≥ 100 ms. More quantitative examination is in progress and will be published elsewhere.

Lastly, we would like to point out that ^{13}C CSA can also be used to broaden the ^{13}C resonances to provide spectral overlap, thus leading to what may be called ^{13}C CSA-assisted rotational resonance (CARR). Reintroduction of CSA under MAS without applying any rf pulses to ^{13}C can most easily be done by spinning a sample at an off magic angle, and 2D polarization transfer experiments can be made by the switching-angle sample spinning (SASS) method.[33,34] Off-magic angle spinning also reintroduces the ^{13}C–^{13}C and ^{13}C–^{1}H dipolar interactions,[35] which would enhance ^{13}C–^{13}C polarization transfer. In fact, SASS has been applied for distance measurement in a doubly ^{13}C-labeled peptide by observing a ^{13}C–^{13}C Pake pattern,[36] for characterization of inhomogeneous solids by observing ^{13}C–^{13}C polarization transfer among different domains,[37] and for cross polarization under MAS.[38] Examination of CARR is undergoing and will be published elsewhere.

ACKNOWLEDGMENT

APPENDIX: CONVENTIONAL VERSUS SECULAR AVERAGING THEORY

In this work, the interference effect of two time-dependent interactions with common Fourier components are examined using either the secular average Hamiltonian theory or the conventional average Hamiltonian theory. Here, we compare these two average Hamiltonian theories using a model Hamiltonian composed of two time-dependent non-commutable interactions,

$$\mathcal{H}(t) = \mathcal{H}_0(t) + \mathcal{H}_1(t)$$

with

$$\mathcal{H}_0(t) = \nu_1 I_x \cos 2\pi \nu_x t$$

and

$$\mathcal{H}_1(t) = \delta I_z \cos(2\pi \nu_z t - \phi). \quad (A1)$$

We may view the former as an amplitude-modulated rf irradiation and the latter as an anisotropic chemical-shift interaction or a heteronuclear dipolar interaction modulated by sample spinning. The evolution of the spin system is described by the propagator $U(t)$,

$$U(t) = T \exp\left\{ -2\pi i \int_0^t dt' \mathcal{H}(t') \right\}, \quad (A2)$$

where T is the Dyson time-ordering operator.

Under the framework of the conventional average Hamiltonian theory, we evaluate $U(t)$ by separating $\mathcal{H}_0(t)$ from $\mathcal{H}_1(t)$ as

$$U(t) = U_0(t) U_1(t), \quad (A3)$$

with

$$U_0(t) = T \exp\left\{ -2\pi i \int_0^t dt' \mathcal{H}_0(t') \right\}$$

$$= \exp\left\{ -i I_x \frac{\nu_1}{\nu_x} \sin(2\pi \nu_x t) \right\} \quad (A4)$$

and

$$U_1(t) = T \exp\left\{ -2\pi i \int_0^t dt' \tilde{\mathcal{H}}_1(t') \right\}. \quad (A5)$$

The Hamiltonian $\tilde{\mathcal{H}}_1(t)$ in the interaction frame defined by $U_0(t)$ is written using the nth Bessel function J_n as

$$\tilde{\mathcal{H}}_1(t) = U_0^{-1}(t)\mathcal{H}_1(t)U_0(t)$$

$$= \delta \cos(2\pi\nu_z t - \phi)$$

$$\times \sum_{n=0,1,\dots} \left[I_z \epsilon_n \cos(4n\pi\nu_x t) J_{2n}\left(\frac{\nu_1}{\nu_z}\right) \right.$$

$$\left. + 2I_y \sin\{(4n+2)\pi\nu_x t\} J_{2n+1}\left(\frac{\nu_1}{\nu_z}\right) \right] \quad (A6)$$

with $\epsilon_0 = 1$ and $\epsilon_{n \geq 1} = 2$. When the two modulation frequencies are matched ($\nu_z = \nu_x = \nu_0$) with each other, Eq. (A6) can be rewritten as

$$\tilde{\mathcal{H}}_1(t) = \delta \sin \phi J_1\left(\frac{\nu_1}{\nu_0}\right) I_y + \text{time dependent terms}, \quad (A7)$$

where the first term represents the zeroth order average Hamiltonian in the interaction frame,

$$\overline{\tilde{\mathcal{H}}_1}^{(0)} = \delta \sin \phi J_1\left(\frac{\nu_1}{\nu_0}\right) I_y. \quad (A8)$$

Note here that at $\tau_0 \nu_0 = n$ (n is an integer number), $U_0(\tau_0) = 1$, and we have

$$U(\tau_0) = U_1(\tau_0) \sim \exp(-2\pi i \overline{\tilde{\mathcal{H}}_1}^{(0)} \tau_0). \quad (A9)$$

The secular averaging Hamiltonian theory can be applied when the two modulational frequencies are matched with each other. In this approach, we represent the total Hamiltonian as

$$\mathcal{H}(t) = H_1 \exp(2\pi i \nu_0 t) + H_{-1} \exp(-2\pi i \nu_0 t) \quad (A10)$$

with

$$H_{\pm 1} = \frac{\nu_1}{2} I_x + \frac{\delta}{2} I_z \exp(\mp i\phi), \quad (A11)$$

and the first order secular average Hamiltonian is given by

$$\bar{H}^{(1)} = \frac{1}{\nu_0}[H_1, H_{-1}]$$

$$= \frac{\delta\nu_1}{2\nu_0} \sin \phi I_y. \quad (A12)$$

It is true that the latter secular average Hamiltonian theory gives us a simpler perspective of interference of two time-dependent Hamiltonians; however, apparently its application should be limited. For example, we intuitively expect decoupling $[\tilde{\mathcal{H}}_1(t) \to 0]$ for $\nu_1 \gg \nu_0$, and in fact, Eq. (A8) calculated using the average Hamiltonian theory predicts decoupling as $\lim_{x \to \infty} J_1(x) \to 0$. On the contrary, Eq. (A12) indicates larger recoupling for larger ν_1. By comparing Eqs. (A8) and (A12), it is noted that the secular average Hamiltonian theory gives proper results only when

$$\frac{\nu_1}{2\nu_0} \sim J_1\left(\frac{\nu_1}{\nu_0}\right) \quad (A13)$$

is satisfied. From Fig. 16, in which $y = J_1(x)$ and $y = \frac{1}{2}x$ for $x = 0-2$ are compared, it is clear that both approaches be-
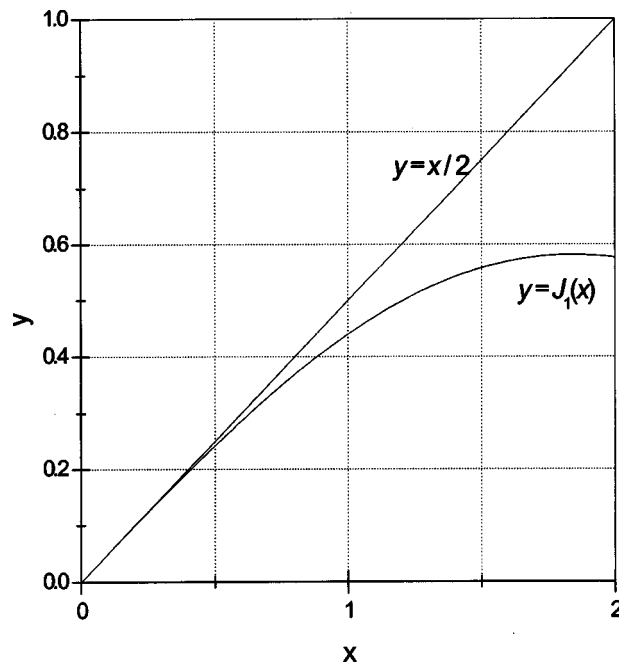

FIG. 16. Comparison of the first Bessel function $J_1(x)$ and $x/2$.

come consistent with each other for $\nu_0 \geq \nu_1$. Similar results have also been deduced for the case of MORE.[24] In the present $^{13}\text{C}-^{13}\text{C}$ recoupling experiments, this denotes that ν_R for the second order DARR [Eq. (37)] or $\nu_R - \nu_{\text{Mod}}$ for RIR [Eq. (47)] should be larger than the size of the heteronuclear dipolar interaction for the secular average Hamiltonian approach to be valid. Otherwise the secular average Hamiltonian overestimates the amount of recoupling.

[1] N. Bloembergen, Physica (Amsterdam) **15**, 386 (1949).
[2] B. H. Meier, Adv. Magn. Opt. Reson. **18**, 1 (1994).
[3] A. E. Bennett, J. H. Ok, R. G. Griffin, and S. Vega, J. Chem. Phys. **96**, 8624 (1992).
[4] N. C. Nielsen, H. Bildsœ, H. J. Jakobsen, and M. H. Levitt, J. Chem. Phys. **101**, 1805 (1994).
[5] J. M. Joers, R. Rosanske, T. Gullion, and J. R. Garbow, J. Magn. Reson. A **106**, 123 (1994).
[6] Y. K. Lee, N. D. Kurur, M. Helmle, O. Johannessen, N. C. Nielsena, and M. H. Levitt, Chem. Phys. Lett. **242**, 304 (1995).
[7] K. Takegoshi, K. Nomura, and T. Terao, Chem. Phys. Lett. **232**, 424 (1995).
[8] E. R. Andrew, S. Clough, L. F. Farnell, T. D. Gledhill, and I. Roberts, Phys. Lett. **21**, 505 (1966).
[9] D. P. Raleigh, G. S. Harbison, T. G. Neiss, J. E. Roberts, and R. G. Griffin, Chem. Phys. Lett. **138**, 285 (1987).
[10] B. H. Meier and W. L. Earl, J. Am. Chem. Soc. **109**, 7937 (1987).
[11] M. G. Colombo, B. H. Meier, and R. R. Ernst, Chem. Phys. Lett. **146**, 189 (1988).
[12] A. Kubo and C. A. McDowell, J. Chem. Soc., Faraday Trans. Part 1 **84**, 3713 (1988).
[13] W. E. J. R. Maas and W. S. Veeman, Chem. Phys. Lett. **149**, 170 (1988).
[14] T. Nakai and C. A. McDowell, J. Chem. Phys. **96**, 3452 (1992).
[15] T. Nakai and C. A. McDowell, Mol. Phys. **88**, 1263 (1996).
[16] For a review, see S. O. Smith, *Encyclopedia of Nuclear Magnetic Resonanance*, edited by D. M. Grant and R. K. Harris (Wiley, Chichester, 1996), Vol. 7, p. 4185.
[17] K. Takegoshi, S. Nakamura, and T. Terao, Chem. Phys. Lett. **307**, 295 (1999).
[18] K. Takegoshi, S. Nakamura, and T. Terao, Chem. Phys. Lett. **344**, 631 (2001).
[19] T. G. Oas, R. G. Griffin, and M. H. Levitt, J. Chem. Phys. **89**, 692 (1988).

[20] K. Takegoshi and T. Terao, Solid State Nucl. Magn. Reson. **13**, 203 (1999).

[21] K. Takegoshi and T. Terao, J. Chem. Phys. **117**, 1700 (2002).

[22] U. Haeberlen and J. S. Waugh, Phys. Rev. **175**, 453 (1968).

[23] M. Mehring, *High Resolution NMR in Solids*, 2nd ed. (Springer, Berlin, 1983), Appendix G.

[24] K. Takegoshi, K. Takeda, and T. Terao, Chem. Phys. Lett. **260**, 331 (1996).

[25] A. Kubo and C. A. McDowell, J. Chem. Soc., Faraday Trans. 1 **84**, 3713 (1988).

[26] K. Takegoshi, D. Reichert, and T. Terao, in Proceedings of the 36th NMR Symposium, Tokyo, 1997, p. 334.

[27] M. Lee and W. I. Goldburg, Phys. Rev. A **140**, 1261 (1965).

[28] T. Gullion and J. Schaefer, J. Magn. Reson. **81**, 196 (1989).

[29] K. Nomura, K. Takegoshi, T. Terao, K. Uchida, and M. Kaisnosho, J. Biomol. NMR **17**, 111 (2000).

[30] M. Baldus and B. H. Meier, J. Magn. Reson. **128**, 172 (1997).

[31] T. Hoshino, A. Kubo, F. Imashiro, and T. Terao, Mol. Phys. **93**, 301 (1998).

[32] M. Hohwy, C. M. Rienstra, C. P. Jaroniec, and R. R. Griffin, J. Chem. Phys. **110**, 7983 (1999).

[33] T. Terao, T. Fujii, T. Onodera, and A. Saika, Chem. Phys. Lett. **107**, 145 (1984).

[34] A. Bax, N. M. Szeverenyi, and G. E. Maciel, J. Magn. Reson. **55**, 494 (1983).

[35] T. Terao, H. Miura, and A. Saika, J. Chem. Soc. **85**, 3816 (1986).

[36] A. C. Kolbert, P. J. Grandinetti, M. Baldwin, S. B. Prusiner, and A. Pines, J. Phys. Chem. **98**, 7936 (1994).

[37] M. Tomaselli, B. H. Meier, M. Baldus, J. Eisenegger, and R. R. Ernst, Chem. Phys. Lett. **225**, 131 (1994).

[38] M. Sardashti and G. E. Maciel, J. Magn. Reson. **72**, 467 (1987).